Collision Risk Assessment of Reduced Aircraft Separation Minima in Procedural Airspaces Using Advanced Communication and Navigation

Qing Cai, Hao Jie Ang, Sameer Alam*
Air Traffic Management Research Institute, School of Mechanical & Aerospace Engineering, Nanyang Technological University, 639798, Singapore
**Corresponding Author: Sameer Alam (Email: sameeralam@ntu.edu.sg)*

Abstract

In order to maintain safety of air traffic operations, stringent aircraft separation standards are in place to reduce mid-air collisions. Note that the separation minima for aircraft flying in a procedural airspace (limited Communication, Navigation and Surveillance (CNS) services) are normally larger than those for a non-procedural airspace. With the advancement of CNS technologies such as space-based Automatic Dependent Surveillance-Broadcast/Contract (ADS-B/C), large separation minima may be reduced in procedural airspaces. It is of great significance to know the upper limit of the Reduced Separation Minima (RSM) for a procedural airspace and the corresponding consequences on collision risk with specifics of the advanced ADS-B and control intervention model. In this work, an interactive software is first developed for collision risk estimation. This software integrates the International Civil Aviation Organization (ICAO) collision risk models for lateral and longitudinal collision risk calculation for the Singapore procedural airspace. Results demonstrates that the lateral and longitudinal collision risk of Singapore procedural airspace with respect to current control procedures meet the ICAO Target Level of Safety (TLS) standard. Moreover, the feasibility of reducing the horizontal separations implemented to the Singapore procedural airspace with respect to advanced CNS techniques is investigated. It is found that if advanced CNS technologies are applied, then the current 50-NM lateral and longitudinal separation standards can be reduced to 22 NM and 20 NM, respectively, to meet the TLS standards based on current demand. A method is then devised to expand the traffic demand by p% based on existing traffic data. Collision risk is then analyzed based on expanded demands by varying p from 10 to 200 to explore the corresponding minimum horizontal separations. It is found that the minimum lateral separation can be reduced from 50 NM to be within the range of [23, 31] NM for $p \in [10, 200]$, while the minimum longitudinal separation can be reduced from 50 NM to 20 NM for $p \in [10, 200]$, while the horizontal collision risk still meets the TLS standards.

Keywords: Air transportation, collision risk, procedural airspace, separation minima, space-based ADS-B

1. Introduction

Given the continued growth in air transportation, one of the key challenges faced by Air Navigation Service Providers (ANSPs) and airlines is: how to increase airspace capacity without compromising on safety? New air traffic management (ATM) paradigms, e.g. European SESAR [1–3] and US NextGen [4, 5], aim for doubling the airspace capacity (2x) while increasing the safety by a factor of 10 by 2030. To achieve such ambitious targets, development of new operational concepts, safety measures and safety performance indicators in the air traffic system are not only expected but also necessary [6–9].

In order to increase airspace capacity so as to accommodate the ever-increasing traffic demand, one of the most effective methods is to reduce the separation standards between aircraft [10]. The en-route airspace, also known as the Reduced Vertical Separation Minimum (RVSM) airspace ranging vertically from 29,000 feet (FL290) to 41,000 feet (FL410), is one of the most heavily congested components of a national airspace system [11–14]. In a RVSM airspace the vertical separation had been reduced from 2000 feet to 1000 feet, adding 6 extra flight levels [15]. A RVSM airspace is preferred by commercial jetliners as it maximizes fuel efficiency, while observing special safety measures, based upon stringent, continuous altitude and track monitoring [14].

With more and more flights flying in RVSM airspaces, the en-route airspaces become more and more congested, leading to potentially higher risk for mid-air aircraft collision [16–18]. Airspace collision risk estimation is a vital indicator for estimating safety in en-route airspaces [19–22]. The collision risk is computed using complex mathematical models involving complex data-set ranging from

aircraft track-data, kinematic data, flying time, CNS parameters etc [20, 23–25]. The model computations are dynamic in nature and includes convolution of statistical distribution of deviations of two aircraft on intersecting and non-intersecting tracks [26–29].

When two aircraft are flying at two intersecting tracks at the same flight level, then controllers will apply horizontal separation minima to segregate the aircraft to avoid loss of separation [30]. It should be pointed out that the horizontal separation minima may vary from sectors to sectors depending on the corresponding CNS capabilities [31]. For a certain Flight Information Region (FIR), its configuration may involve procedural airspaces. A procedural airspace is an airspace volume in which the air traffic control services are provided without the use of radar. Procedural airspaces are normally planned for sparsely populated land areas and oceans, where radar coverage is either prohibitively expensive or is simply not feasible. Due to the limited CNS services in procedural airspaces, larger horizontal separation minima (eg., 30 NM or 50 NM longitudinal and 30 NM or 50 NM lateral separation minima in Santa Maria Oceanic control area over the Atlantic Ocean) had been implemented in procedural airspaces as compared to that of non-procedural airspaces.

With the advancement of CNS technologies especially space-based ADS-B and Global Navigation Satellite System (GNSS) [32–34], flights flying in procedural airspace are better monitored and have improved navigation performance. As a consequence, such large horizontal separation minima in procedural airspace may be further reduced to increase the airspace capacity and save fuel burning [18, 35] non compromising safety. For example, a 50 NM instead of 100 NM lateral separation had been adopted in the South Atlantic FIRs [36]. Many ANSPs are considering to reduce the separations in procedural airspaces. See the VOICE project funded by SESAR JU for more information. Note that the reduction on separation minima is likely to increase the collision risk for the traffic within a given procedural airspace. Collision risk estimation is pertaining to both airspace structure management and air traffic flow management [19, 22, 37–39]. According to the ICAO circular 319 ‘the purpose of collision risk models in the context of the determination of separation minima is to model the chain of events leading a pair of initially separated aircraft to a collision’ [40].

Scientists have proposed several mathematical models for collision risk estimation [21, 28, 41–43]. However, those collision risk models are mathematically complicated and they were developed based upon old CNS technologies. If new RSM are implemented in a given procedural airspace, it is not known how the RSM will affect the traffic safety as well as the efficiency of the given airspace. As a consequence, before new RSM are to be implemented to a procedural airspace, the following four key research questions need to be answered.

- First, what is the baseline collision risk for the air traffic within a given procedural airspace under current CNS services?
- Second, how to model advanced CNS services and RSM in the existing collision risk models for procedural airspace?
- Third, what are the collision risk parameters and the upper limits of the RSM that can be achieved while maintaining the TLS of the airspace with respect to current traffic demand?
- Fourth, what are the collision risk parameters and the upper limits of the RSM that can be achieved while maintaining the TLS of the airspace with respect to increased future traffic demand?

This paper attempts to answer the above four questions. The answers can help ANSPs to build a holistic view of the safety assessment of their FIRs. Meanwhile, the corresponding research findings can be used as a reference by ANSPs to manage/improve the configurations of procedural airspaces in terms of separation standards, ATS route structures, air traffic flow management protocols, CNS technologies, etc. The main contributions of this paper are highlighted as follows:

- A collision risk modelling and simulation software is developed with interactive and visualization capabilities. This software is named CREAM. The CREAM software integrates the ICAO models for collision risk computation and analysis. The CREAM software is able to provide visual clues regarding the collision risk at given waypoints and airway segments for decision makers.

- The horizontal collision risk of the procedural airspace of Singapore FIR is analyzed using the CREAM software with respect to current control procedures and traffic demand. Experimental results show that the lateral and longitudinal collision risk of Singapore procedural airspace meets the ICAO TLS standard.
- The feasibility of reducing the horizontal separations, that are currently implemented to the Singapore procedural airspace, with respect to advanced CNS techniques is investigated. Experimental results shows that the 50-NM lateral and longitudinal separation standards applied to the Singapore procedural airspace can be respectively reduced to 22 NM and 20 NM with respect to current demand, while the collision risk still meets the TLS standards.
- A method is proposed to expand the traffic demand by $p\%$ based on existing traffic data. The collision risk is then analyzed based on the expanded demands by varying p from 10 to 200 to explore the corresponding minimum horizontal separations. It is found that the minimum lateral separation can be reduced from 50 NM to be within the range of [23, 31] NM for $p \in [10, 200]$, and the minimum longitudinal separation can be reduced from 50 NM 20 NM for $p \in [10, 200]$, while the horizontal risk still meets the TLS standards.

The remainder of this paper is organized as follows. Section 2 provides the preliminaries for a better understanding of this research. Section 3 describes amply the research methodology. Section 4 displays the experimental settings. Section 5 demonstrates the case study on Singapore airspace, including the baseline collision risk analysis using the CREAM software, the feasibility of separation reduction and its impact on collision risk with respect to current and future traffic demand. Section 6 concludes the paper.

2. Preliminaries

For a smooth reading of this paper, this section provides some basic knowledge. These knowledge include aircraft separation standards, collision risk definition, and ICAO mathematical models for collision risk estimation.

2.1 Aircraft Separation Standard

Due to the growing demands of the air traffic in upper airspace and the need for more fuel efficient flight levels, ICAO, in 1982, had introduced the concept of RVSM which decreases the vertical separation minimum from 2000 feet (Conventional Vertical Separation Minimum – CVSM) to 1000 feet (RVSM) for aircraft operating at FL 290 to FL 410.

Apart from vertical separation standard, aircraft are also separated by horizontal separation standards, namely lateral separation and longitudinal separation. A typical 50-NM lateral separation and a 50-NM longitudinal separation are applied to the Singapore procedural airspace. Note that the exact separation standards are dependent on the specific CNS technologies. More details about the separation standards under various scenarios can be found in the ICAO documents in [30, 31, 44].

2.2. Collision Risk

In all regions where RVSM has been implemented, Regional Monitoring Agencies (RMAs) have been established by the appropriate Planning and Implementation Regional Groups (PIRGs) to satisfy the goals of the RVSM monitoring program. It is an RMA's duty and responsibility to provide annual reports to the PIRG to report the assessment of the collision risk in the system against the overall safety objectives to support the continued safe use of the RVSM.

According to ICAO, collision risk is defined as "the expected number of mid-air aircraft accidents in a prescribed volume of airspace for a specific number of flight hours due to loss of planned separation". Collision risk provides a holistic view for the safety level of the traffic within a given airspace for a given period of time.

Based on ICAO regulation, there are two specific safety objectives for collision risk assessment, namely an assessment of the technical vertical risk against a TLS of 2.5×10^{-9} fatal accidents per flight hour (fapfh), and an assessment of the total vertical risk against a TLS of 5×10^{-9} fapfh [45]. The horizontal risk that consists of lateral risk and longitudinal risk is also assessed against a TLS of 5×10^{-9} fapfh. According to FAA, the 2015 annual flight hours for the USA was 9.8 million flight

hours. Therefore, a vertical TLS of 5×10^{-9} fapfh equates to an acceptable value of risk of roughly 1 fatal accident every 20 years resulting from a loss of vertical separation.

2.3. Horizontal Collision Risk Models

This section presents the concise forms of the mathematical models developed by ICAO for horizontal collision risk estimation. More mathematical details pertaining to the horizontal collision risk models can be found in the Appendix. Interested readers are also encouraged to refer to materials in [31, 40, 46–48].

2.3.1. Key Parameters and Definitions

Before presenting the horizontal collision risk models, all the related parameters are first summarized. Table 1 lists out the definitions of the key parameters pertaining to the horizontal collision risk models.

Table 1:Definitions of the parameters involved in the collision risk models. See refs. [28, 40, 49] for more details.

Parameter	Definition
N_{ay}	Expected number of accidents (two per each aircraft collision) per flight hour due to the loss of lateral separation between aircraft flying on tracks with nominal spacing S_y
N_{ax}	Expected number of accidents (two per each aircraft collision) per flight hour due to the loss of longitudinal separation between aircraft flying on a track with nominal spacing S_x
S_x, S_y	Minimum standard longitudinal and lateral separations
S_X	Length of the longitudinal window used in the calculation of occupancies
$P_y(S_y)$	Lateral overlap probability of aircraft nominally flying on laterally adjacent paths at the same FL
$P_z(0)$	Vertical overlap probability of aircraft nominally flying at the same FL
$HOP(t \mid V_1, V_2)$	Horizontal overlap probability for a pair of aircraft during time interval $[t_0, t_1]$ given speeds V_1 and V_2
$E_y(same), E_y(opp)$	Same direction and opposite direction lateral occupancies, i.e. the average number of same direction and opposite direction aircraft flying on laterally adjacent tracks at the same FL within segments of length $2S_x$ centred on the typical aircraft
$\lvert\bar{V}\rvert$	Average ground speed of the aircraft
$\overline{\lvert\dot{y}(S_y)\rvert}$	The average lateral cross-track speed between aircraft that have lost their lateral separation
$\overline{\lvert\dot{z}\rvert}$	The average relative vertical speed of aircraft flying at the same FL
$\overline{\lvert\dot{x}\rvert}$	The average relative along-track speed of aircraft flying at the same FL in the same direction
$\lambda_x, \lambda_y, \lambda_z$	The average length, width and height of a typical aircraft using the rectangular box model
λ_{xy}	The average diameter of a cylinder modelling a typical aircraft
$D_x(t)$	Distance between the two aircraft
λ	The scale parameter of the along-track and cross-track navigation error
λ_v	Scale factor for speed error distribution
V_r	Relative velocity
NP	No of a/c per hour
t_0, t_1	ADS periodic report time interval
T	ADS periodic report time
τ	Controller intervention buffer
$f_1(V_1)$	Distribution of aircraft speed

Keeping in mind all the key parameters as listed out in Table 1, we briefly elucidate in what follows the probabilistic models for estimating lateral and longitudinal risk.

2.3.2. Lateral Collision Risk Model

The probabilistic model that is used for calculating the lateral collision risk for parallel tracks can be written as

$$N_{ay} = P_y(S_y)P_z(0)\frac{\lambda_x}{S_X}\left\{E_y(same)\left[\frac{\overline{|\dot{x}|}}{2\lambda_x}+\frac{\overline{|\dot{y}(S_y)|}}{2\lambda_y}+\frac{\overline{|\dot{z}|}}{2\lambda_z}\right]+E_y(opp)\left[\frac{|\overline{V}|}{\lambda_x}+\frac{\overline{|\dot{y}(S_y)|}}{2\lambda_y}+\frac{\overline{|\dot{z}|}}{2\lambda_z}\right]\right\} \quad (1)$$

2.3.3. Longitudinal Collision Risk Model

The longitudinal risk within the time interval $[0, T_i]$ with respect to a certain longitudinal separation S_j is calculated as

$$N_{ax}(S_j, T_i) = 2NP\int_{-\infty}^{\infty}\int_{-\infty}^{\infty}\int_{t_0}^{t_1} HOP(t|V_1, V_2)P_z(h_z)\left(\frac{2V_r}{\pi\lambda_{xy}}+\frac{\overline{|\dot{z}|}}{2\lambda_z}\right)f_1(V_1)f_2(V_2)dtdV_1dV_2 \quad (2)$$

2.3.4. Discussions

In equations 1 and 2, there are several key components, i.e., $P_y(S_y)$, $P_z(0)$, $E_y(same)$, $E_y(opp)$, $HOP(t|V_1, V_2)$, $f_1(V_1)$ and $f_2(V_2)$. The modelling and calculations of those components are delineated in the Appendix.

There are two types of collision risk, i.e., vertical and horizontal risk. However, this research will only focus on the horizontal risk, i.e., lateral and longitudinal risk. The reason is that the purpose of this paper is to investigate the feasibility of RSM and its impact on airspace safety in terms of collision risk.

Regarding the RSM, only reduced horizontal separation will be analyzed while RVSM is not considered. This is because that an aircraft is subject to the Total Vertical Error (TVE) – difference between the actual altitude flown and the assigned pressure altitude – which is mainly captured by the Altimetry System Error (ASE) – difference between the instrument displayed pressure altitude and actual altitude flown – and the Assigned Altitude Deviation (AAD) – difference between assigned altitude and the altitude flown transponded or provided from the aircraft equipment. The tolerances for ASE and AAD are 245 ft and 300 ft, respectively, leading to the tolerance for TVE being 300 ft (see references FAA Advisory Circular, No 91-85B and ICAO EUR Doc 009, version 3, for more information). Consequently, it is very challenging to further reduce the RVSM of 1000 ft. Meanwhile, the 1000 ft vertical separation standard has been verified to be fuel friendly and operationally safe [14].

3. Research Methodology

This section is divided into seven subsections. The first subsection presents an overview of the research methodology. The second subsection gives a brief introduction to the CREAM software. The third and fourth subsections show how the collision risk models which are currently used by ANSPs can be adopted to estimate collision risk with RSM and advanced CNS techniques. The fifth subsection illustrates how we derive the initial longitudinal separation distributions for subsequent longitudinal collision risk calculation. The sixth subsection explicitly summarizes the research assumptions that we have made in this research. The last subsection describes the proposed method for simulate future traffic demand based on current one.

3.1. Methodology Overview

As mentioned in the introduction section, this research aims to answer four research questions. Fig. 1 presents a concept diagram of the proposed methodology for seeking answers to the four research questions.

As can be seen from Fig. 1, collision risk calculation for a given procedural airspace is non-trivial as it is involved not only with data pre-processing and analytics for several types of input data such as traffic sample data, aircraft performance data, airway information, etc., but also with the understanding and adoptions of mathematical collision risk models. Meanwhile, it is difficult to measure the resultant impact of RSM in a procedural airspace with respect to advanced CNS on the corresponding collision risk.

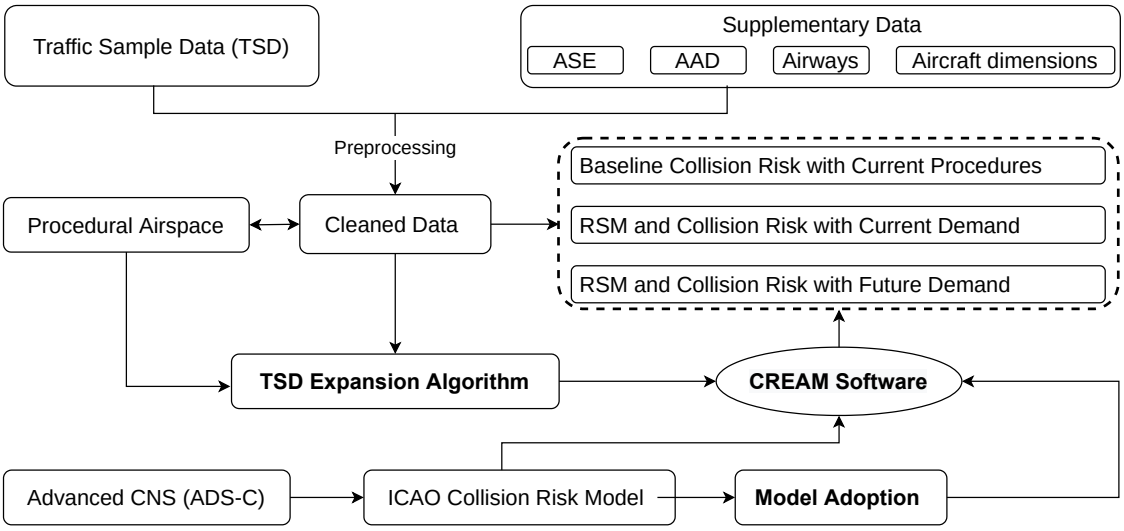

Figure 1: Concept diagram of the proposed methodology for seeking answers to the research questions.

In this work, we aim to overcome the above challenges through three key steps: development of a software for collision risk calculation; adoption of ICAO collision risk models to account for advanced CNS; simulation of future traffic demand by expanding current traffic scenario. Those three steps will be elucidated amply in what follows.

3.2. The CREAM Software

CREAM is a software developed by the authors using Python programming language. In what follows we present a brief introduction to the CREAM software in terms of software framework, software interface demonstration and collision risk estimation validation on Singapore FIR.

3.2.1. Framework of CREAM

Fig. 2 presents the framework of the CREAM software. As can be seen from the central part of Fig. 2, the CREAM software has two core modules, i.e., collision risk estimation module and collision risk management module. The estimation module adopts the ICAO models for collision risk estimation, while the management module integrates data-driven approaches developed by the authors for collision risk mitigation.

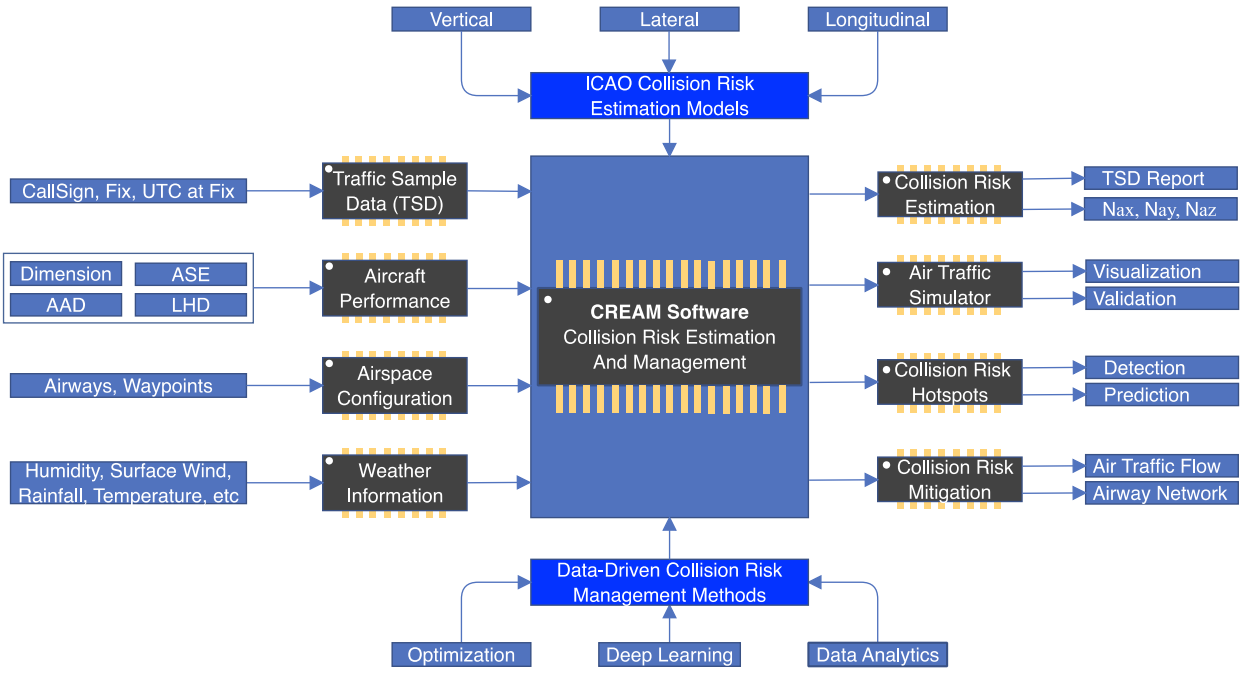

Figure 2: Framework of the CREAM software for air traffic collision risk estimation and management.

CREAM can be used to estimate the collision risk of the en-route traffic within any given FIR (default) or an airspace region, as long as the airspace configuration data, aircraft performance data and the corresponding traffic data can be provided to the software. It is able to estimate air traffic collision risk in three different planes, i.e., vertical, lateral, and longitudinal planes (N_{ax}, N_{ay}, N_{az} as shown on the righthand side of Fig. 2). Regarding the risk estimation, the software can provide a basic report for the traffic data. Meanwhile, as can be seen from Fig. 2, CREAM is also equipped with the component Air Traffic Simulator. This simulator contains two functionalities, i.e., visualization and validation. The visualization functionality is oriented to air traffic movement visualization and collision risk visualization (at given waypoints and airway segments), thereby providing visual clues to assist decision makers with a better understanding of the estimated collision risk. The validation functionality mainly helps with a fast simulation of traffic control protocols aiming for improving the traffic safety. For example, when the visual clues indicate that the collision risk at a certain area is relatively higher than other areas, then traffic planners can modify the traffic data to simulate the traffic management interventions made by means such as flight level change, vectoring, speed control, and so on. Once a new traffic data is obtained, then users can easily upload the data to the CREAM software to recalculate the resultant collision risk to validate if the traffic management interventions can reduce the collision risk or not. Meanwhile, the software is also integrated with the functionality of collision risk hotspot analysis. This functionality deals with collision risk hotspot detection and prediction. Collision risk hotspot detection helps decision makers to locate airspace regions that witness high collision risk, while hotspot prediction helps decision makers to get to know the possible airspace regions that will suffer from high collision risk in the near future such that decision makers can take pre-caution measures.

Regarding the collision risk management, CREAM is integrated with a couple of risk mitigation solutions which can be categorized into two groups, i.e., traffic flow management and airway network structure management. The traffic flow management solutions aim to manage the traffic in terms of flight plans, aircraft speeds, and flights' assigned levels, in such an optimal way that the overall risk can be further reduced. The airway network structure management solutions aim to optimize the structure of a given airway network such that the vertical and/or horizontal overlap between the en-route aircraft can be reduced which then will lead to the reduction of collision risk. When designing data-driven approaches for collision risk management, a promising direction is to do partial flow and/or airway structure management by referring to the collision risk hotspot analysis results. For a given airspace, there could be only several sub-regions suffering from high risk. Therefore, management of traffic flows and the airway structures within those sub-regions could be computationally and operationally friendly. Last but not least, facilitated by the CREAM software, a solution aiming for risk mitigation can be tested through the software.

3.2.2. Demonstration of CREAM

The CREAM software in its current version exempts aviation decision makers from playing with obscure mathematical equations and tedious data pre-processing efforts. The CREAM software can automatically do the data pre-processing and calculate the three types of collision risk. Fig. 3 shows a snapshot of the main interface of the CREAM software.

In the top-left corner of Fig. 3, the TSD is short for Traffic Sample Data and it is the most important data required for the collision risk estimation process. The supplementary data (Suppl as shown in the interface) includes the waypoints, aircraft dimensions, ASE parameters, AAD samples and LHD occurrences and these data are used to estimate the parameters involved in the collision risk models. In the bottom-left corner of the interface, the software visualizes the values of the key parameters involved in the collision risk models. Users can make a coarse comparison between the estimated values against those for other airspaces. Meanwhile, the software also allows users to tune the parameters and recalculate the risk. On the left hand side of the interface, users can click the shaded boxes showing the values of the key parameters involved in the collision risk models to change their values. Then users

can hit the 'Recompute' button to get the new collision risk value. By doing so, users can get to know which parameters impact the most the collision risk. This helps users to draw inspirations for their subsequent measures for traffic management and risk mitigation.

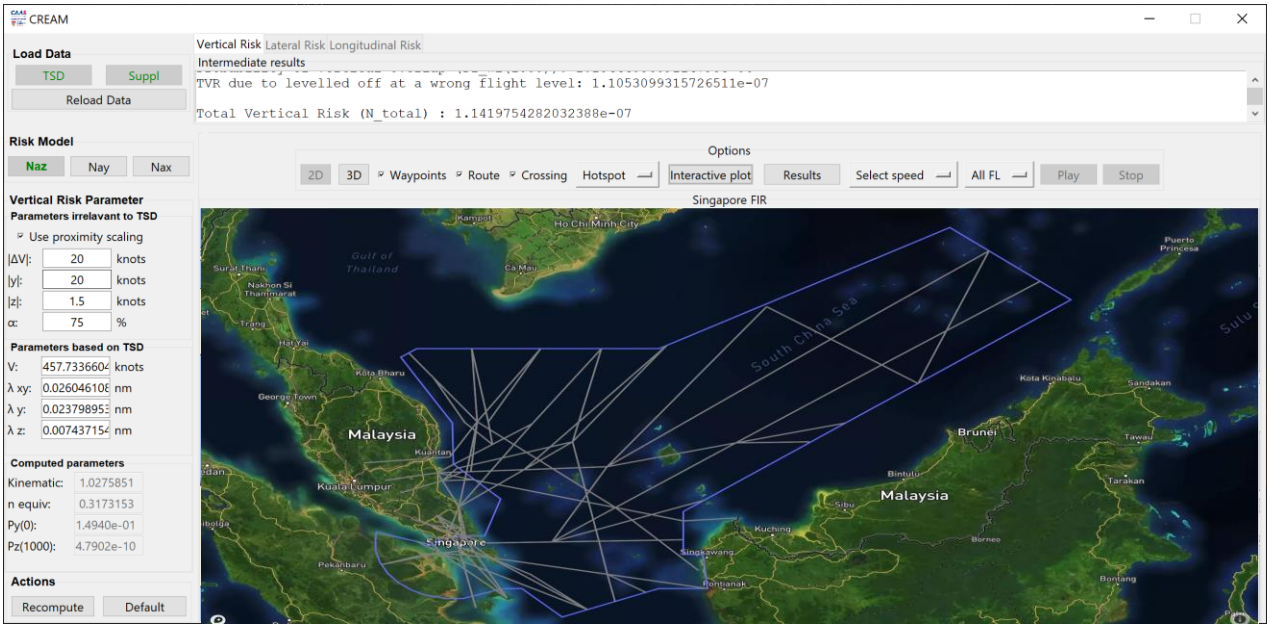

Figure 3: Demonstration of the main interface of the CREAM software.

In the upper-middle part of the interface, there are three icons, i.e., 'Vertical Risk', 'Lateral Risk', and 'Longitudinal Risk', which enable users to switch between them to see all the related information regarding the corresponding risk calculation. Those information includes all the intermediate results and the finally estimated risk, and is shown in the window below those icons. Note that users can fold up and unfold the window for better visualization of the results. Apart from the window, the software also generates external files storing all the related results.

At the bottom of the right hand side of the interface, it presents visual clues pertaining to the collision risk. Those include the 2D and 3D visualizations of the traffic movement, the crossing points pertaining to the vertical risk, collision risk at given waypoints and airway segments. Those clues help aviation decision makers to draw inspirations to do air traffic flow management or even airspace configurations with the aim being improving traffic safety and airspace utilization. Note that the visualizations can be controlled using the options provided in the middle of the right hand side of the interface. The option button "Interactive Plot" will open an external window to better visualize the structure of a given airspace and the corresponding collision risk.

3.2.3. Validation of CREAM

In what follows we present a validation of the software for collision risk estimation. Without loss of generality, here we show the technical vertical collision risk estimation for Singapore airspace. Technical vertical risk is the risk of collision between aircraft that are on adjacent flight levels due to normal or typical height deviations of RVSM approved aircraft. We compare the values of the key parameters obtained using CREAM against those reported by other ANSPs in ICAO documents.

Table 2:Validation of the CREAM software for technical vertical collision risk estimation for Singapore airspace by comparing the values of the key parameters obtained by CREAM against those reported by other ANSPs. Parameter α denotes the portion of aircraft using GNSS navigation.

Parameters for Vertical Risk	Values Obtained by CREAM	Values Reported in ref. [46]	Values Reported in ref. [50]	Values Reported in ref. [51]
λ_x	0.0261 NM	0.0286 NM	0.0308 NM	0.0279 NM

λ_y	0.0236 NM	0.0269 NM	0.0274 NM	0.0254 NM
λ_z	0.0074 NM	0.0084 NM	0.0085 NM	0.0081 NM
λ_{xy}	0.0261 NM	0.0286 NM	0.0308 NM	0.0279 NM
S_z	1000 ft	1000 ft	1000 ft	1000 ft
$\bar{V}$	460.37 knots	464 knots	480 knots	480 knots
$\lvert\overline{\Delta V}\rvert$	20 knots	20 knots	38.3 knots	28.9 knots
$\overline{\lvert\dot{y}\rvert}$	20 knots	20 knots	5 knots	11.6 knots
$\overline{\lvert\dot{z}\rvert}$	1.5 knots	1.5 knots	1.5 knots	1.5 knots
$P_z(S_z)$	1.43×10^{-10}	1.0×10^{-9}	3.6×10^{-8}	1.7×10^{-8}
$P_y(0)$ $(\alpha = 0.75)$	0.1493	0.1060	0.1080	0.0719
$n_z(equiv)$	0.3566 (FIR 1)	0.1241 (FIR 2)	0.2294 (FIR 3)	0.1407 (FIR 4)
N_{az}^T	1.56×10^{-11} fapfh	2.7×10^{-11} fapfh	1.79×10^{-9} fapfh	3.5×10^{-10} fapfh

FIR 1 – Singapore Airspace; FIR 2 – Africa Indian Ocean Airspace; FIR 3 – Pacific Airspace; FIR 4 – Japan Airspace

The vertical collision risk consists of two basic factor which include the likelihood of the loss of vertical separation (reflected by parameter $P_z(S_z)$) and the exposure to the loss of vertical separation (reflected by parameter $n_z(equiv)$). Table 2 presents the comparison results. Note that the values of the parameters obtained by CREAM are based on the TSD for December 2018. In Table 2, most of the parameters can be referred to Table 1. We use N_{az}^T to denote the technical vertical collision risk. More information regarding the technical vertical risk can be found in [20, 52].

As can be seen from Table 2, the values of the kinematic parameters (aircraft dimensions, aircraft speeds) as obtained by CREAM are quite close to those reported by other ANSPs. The values of $P_y(0)$ are also close to each other. However, the values of $P_z(S_z)$ and $n_z(equiv)$ differ a lot which then leads to the difference of the eventual risk N_{az}^T. The differences are due to the specific airspace configurations and traffic flow management. For the four airspaces reported in Table 2, their technical vertical risk are all below the ICAO TLS of 2.5×10^{-9} fapfh.

3.3. Adoption of the Lateral Risk Model

When RSM with respect to advanced CNS technologies are employed to a procedural airspace, the collision risk models shown in the above section need to be adopted to comply with advanced CNS technologies. This section shows how the models are adopted for collision risk estimation with respect to RSM for procedural airspace.

When a reduced lateral separation standard is implemented to a procedural airspace, the following adoptions need to be considered regarding the lateral collision risk model:

1) S_y: The parameter S_y needs to be updated with the reduced lateral separation minimum. The new separation minimum will affect the calculation of the lateral overlap probability $P_y(S_y)$.

2) RNP: The RNP specification needs to be updated to enable reduced lateral separation minimum. The new RNP specification will affect the estimation of the probability distribution of aircraft lateral deviation, eventually affecting the calculation of $P_y(S_y)$.

3.4. Adoption of the Longitudinal Risk Model

When a reduced longitudinal separation standard is implemented to a procedural airspace, the following adoptions need to be considered:

1) RNP: The RNP specification needs to be updated to enable reduced longitudinal separation minimum. In this study, RNP 4 is considered as this RNP specification has been adopted by many procedural airspaces.

2) S_x: The parameter S_x needs to be updated to calculate the horizontal overlap probability.

3) The Intervention Model: Note that the calculation of the longitudinal risk heavily depends on the model used to describe controller intervention to resolve a conflict. The intervention model accounts

for surveillance latency, controller and pilot responses, and aircraft trajectory change. With advanced CNS techniques, the intervention model needs to be adopted.

3.4.1. Longitudinal Risk Based on Existing Intervention Model

Currently, the widely used intervention model for longitudinal risk estimation with respect to existing CNS techniques considers the following three scenarios. See ICAO manual 10120 for more information.

Scenario A: The ADS-C report is delivered to the ATC, which happens with a probability P_S^Y, and the ATC successfully communicates with the pilot via Controller Pilot Data Link Communication (CPDLC) within a maximum transaction time of τ_A minutes, which happens with a probability P_C^Y.

Scenario B: The ADS-C report is delivered to the ATC which happens with a probability P_S^Y, and the ATC failed to communicate with the pilot via CPDLC which happens with a probability P_C^N, but successfully gets in touch with the pilot using high frequency radio within a maximum transaction time of τ_B minutes.

Scenario C: The ADS-C report is not delivered to the ATC which happens with a probability P_S^N, and the ATC communicates with the pilot via high frequency radio within a maximum transaction time of τ_C minutes.

Based on the above three scenarios, the longitudinal risk for a given spacing $S_j \in [S_x, S_x + 250]$ is estimated as

$$N_{ax}(S_j) = {P_S}^Y \cdot {P_C}^Y \cdot N_{ax}(S_j, T_A) + {P_S}^Y \cdot {P_C}^N \cdot N_{ax}(S_j, T_B) + {P_S}^N \cdot N_{ax}(S_j, T_C) \quad (3)$$

in which $T_A = T + \tau_A$, $T_B = T + \tau_B$ and $T_C = T + \tau_C$ with T being the periodic reporting interval.

Note that the existing intervention model is based on the RCP (Required Communication Performance) Communication and Surveillance Timing Model (RCSTM) developed for ATS surveillance separation using RCP 240 communications and ADS-B, and modified to account for differences between ADS-B and ADS-C. Fig. 4 graphically exhibits the detailed intervention model that is being used by many ANSPs.

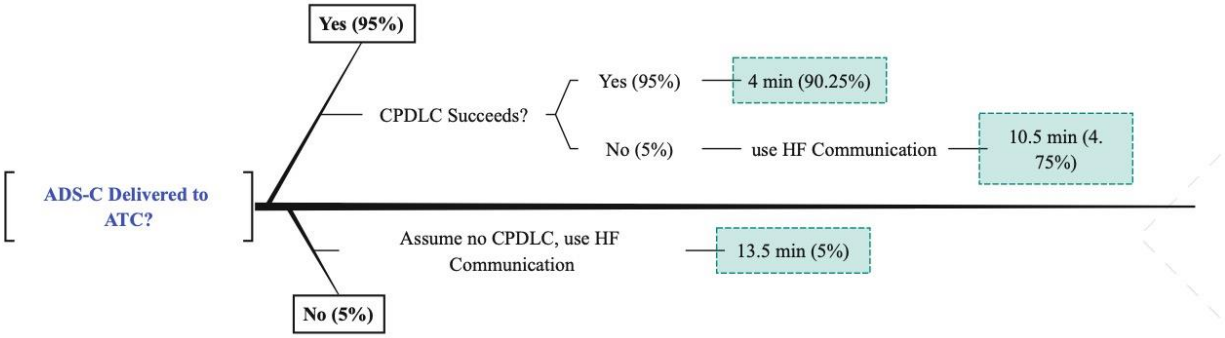

Figure 4: Illustration of the currently used intervention model for longitudinal risk calculation. In the intervention model, three scenarios are considered. Each scenario happens with a certain probability and a specific buffer time as shown in the figure.

According to what is shown in Fig. 4, the longitudinal risk $N_{ax}(S_j)$ can be rewritten as

$$\begin{aligned} N_{ax}(S_j) &= {P_S}^Y \cdot {P_C}^Y \cdot N_{ax}(S_j, T_A) + {P_S}^Y \cdot {P_C}^N \cdot N_{ax}(S_j, T_B) + {P_S}^N \cdot N_{ax}(S_j, T_C) \\ &= 0.95 \times 0.95 \times N_{ax}(S_j, T + 4) + 0.95 \times 0.5 \times N_{ax}(S_j, T + 10.5) + 0.05 \times N_{ax}(S_j, T + 13.5) \\ &= 0.9025 \times N_{ax}(S_j, T + 4) + 0.0475 \times N_{ax}(S_j, T + 10.5) + 0.05 \times N_{ax}(S_j, T + 13.5) \end{aligned} \quad (4)$$

3.4.2. Longitudinal Risk Based on New Intervention Model

The intervention model shown above only considers three scenarios. With advanced CNS techniques, a new intervention model that is able to capture all possible scenarios related to Performance Based Communication and Surveillance (PBCS) is needed.

According to the ICAO manual [48], a new intervention model was suggested. The new intervention model totally consists of 48 scenarios. Each scenario happens with a probability P_i with the intervention time being τ_i. Based on the new model, the calculation of the longitudinal risk for a given spacing $S_j \in [S_x, S_x + 250]$ is updated as

$$N_{ax}(S_j) = \sum_{i=1}^{48} P_i \times N_{ax}(S_j, T + \tau_i) \qquad (5)$$

Fig. 5 demonstrates the new intervention model with details for the 48 scenarios. As can be seen from Fig. 5, the 48 scenarios can be categorized into three main branches, viz., ADS-C nominal, ADS-C failure followed by successful resend and ADS-C failure twice, each of which has branches for communication via CPDLC or High Frequency (HF) radio.

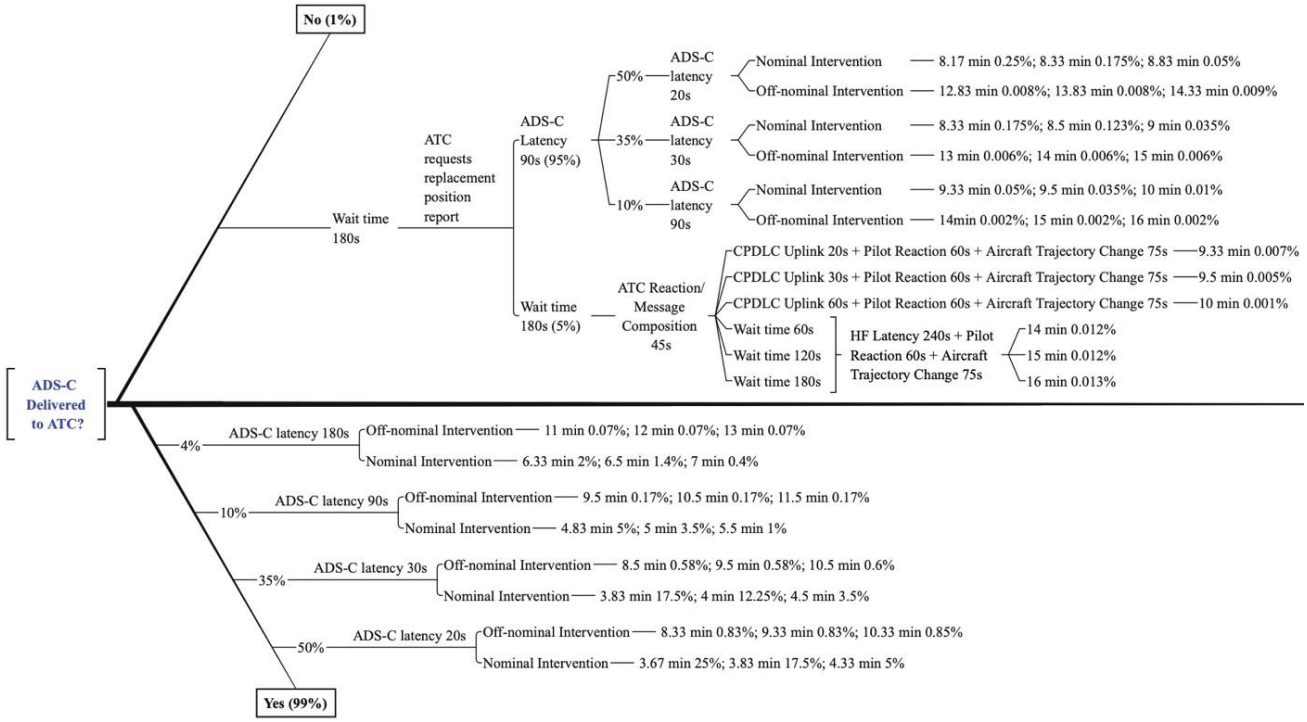

Figure 5: Illustration of the new intervention model for longitudinal risk estimation. In the new intervention model, 48 scenarios are considered. Each scenario happens with a certain probability and a specific buffer time as shown in the figure.

The intervention time τ_i ranges from 3.67 min to 16 min as can be seen from Fig. 5. When calculating $N_{ax}(S_j)$one needs to substitute τ_i together with the corresponding probability P_i into the above equation.

After getting $N_{ax}(S_j)$, the final longitudinal risk is calculated as

$$N_{ax}(S_j) = \sum_{S_x}^{S_x+250} P(S_j) \times N_{ax}(S_j) \qquad (6)$$

in which $P(S_j)$ is the probability for the separation to be S_j.

3.5. Longitudinal Separation Distribution Derivation

For the estimation of longitudinal risk, we need to know the initial longitudinal spacing distribution of the aircraft. Different distributions will lead to different longitudinal risk estimations. In this study we consider three cases pertaining to the initial longitudinal spacing distribution of the aircraft and those cases are elucidated below.

3.5.1. Case 1 – Uniform Distribution

In case 1, we take it that the initial longitudinal separation follows a uniform distribution with the separation ranging from the minimum separation of S_x NM to the maximum separation of $(S_x + 250)$ NM. Studies carried out by the ICAO Separation and Airspace Safety Panel (SASP) showed that a uniform distribution of the initial longitudinal separation yields a far higher risk than any reasonable gamma distribution [48]. This is due to the rapid, approximately exponential decay in risk with distance. Thus, case 1 will lead to a conservative estimation of the longitudinal risk. This suggests that it might be possible to reduce the longitudinal separation standard further with a close monitoring of aircraft spacings and use of a more realistic spacing distribution.

3.5.2. Case 2 – At the Entry Fix

In case 2, we derive the separation distribution from the TSD. Specifically, we derive the distribution based on the FIR entry fix and entry time. The key idea of case 2 involves three steps: First, for a cleaned TSD, all the flights are sorted based on their entry flight levels in an ascending order from FL 290 to FL 410; Second, their entry times are sorted in an ascending order (earliest to latest) with respect to each flight level; Third, the longitudinal separations of aircraft pairs are determined. More specifically, for a given sequence of aircraft at a certain flight level, the time duration between the aircraft first entering the FIR and the subsequent aircraft is determined. Then the separation between those two aircraft is obtained by multiplying the speed of the subsequent aircraft with the obtained time duration.

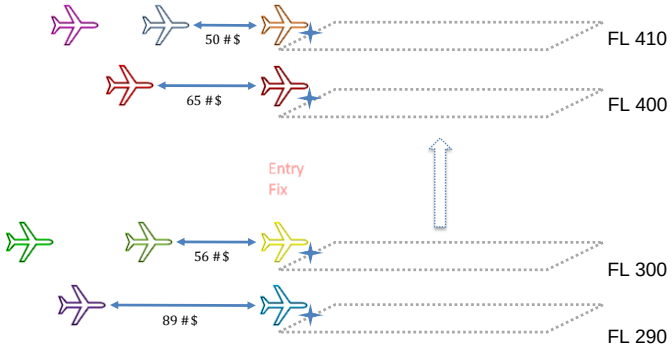

Figure 6: An example of case 2 for deriving the longitudinal separations between aircraft from the TSD.

Fig. 6 gives a graphical example of case 2 for deriving the longitudinal separations. As shown in Fig. 6, aircraft at each FL are sorted based upon their entry times. Then the longitudinal separation between two adjacent aircraft (one at the entry fix and the other is about to reach the entry fix) at a certain FL can be obtained, such as the 50 NM and 65 NM separations as shown in Fig. 6. The above process applies to the entire TSD and a sequence of longitudinal separations is therefore obtained.

3.5.3. Case 3 – After the Entry Fix

Case 3 can be viewed as the extension of case 2. Based on case 2, in case 3 we determine the separations for aircraft within a FIR. After sorting the flights as what have been done in case 2, a time window of δ minutes is adopted to watch the traffic movements. Then the temporal separations are determined. Fig. 7 illustrates the key idea of case 3 with $\delta = 5$ for flights flying at FL 350. As shown in Fig. 7, the yellow aircraft reaches the entry fix at 8:00 AM. For a given time period of 15 minutes with $\delta = 5$, two separations, i.e., 56 NM and 60 NM, are observed.

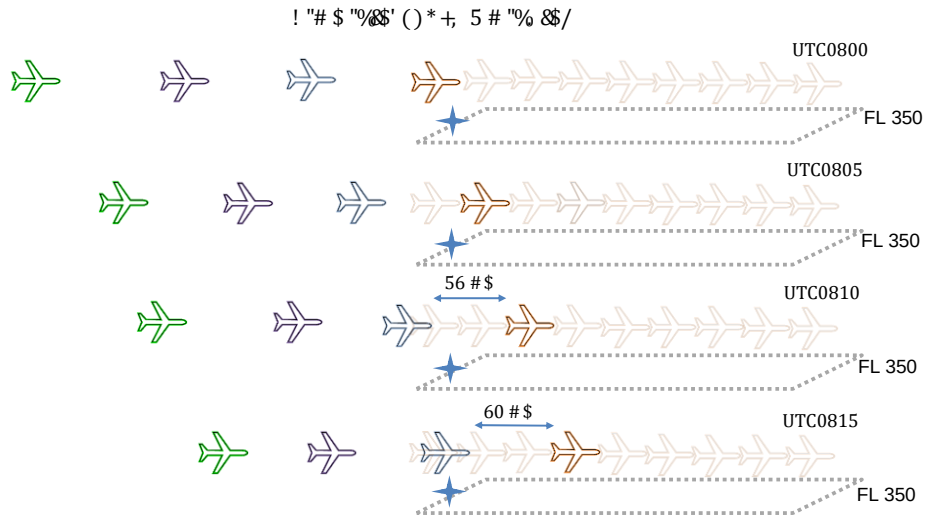

Figure 7: Illustration of the key idea of case 3 for deriving the longitudinal separations with an observation time window of 5 minutes for aircraft flying at FL 350.

In case 3, the longitudinal separations are observed within the FIR. The time window δ is a critical parameter for determining the separation distribution. Therefore, multiple time windows are needed to analyze their impact on the collision risk. In this study, six time windows, i.e., 1 min, 3 min, 5 min, 10 min, 15 min and 20 min, have been adopted. Note that the shortest length of the four studied routes is 204 NM. Therefore, δ cannot be too large. Because if so, then many flights will fly over the procedural airspace (the averaged speed is around 480 knots) and traffic observation samples would be reduced, eliciting inaccurate estimation of the longitudinal separation distribution.

As mentioned earlier, case 1 is more conservative than cases 2 and 3 for longitudinal calculation. In order to calculate the longitudinal risk in a more conservative way, we only integrate case 1 into the CREAM software. However, longitudinal risk with respect to those three cases are all analyzed in this study for research purpose.

3.6. Research Assumptions

When calculating the horizontal collision risk, we need to calculate the components $P_y(S_y)$, $P_z(0)$, $E_y(same)$, $E_y(opp)$, $HOP(t|V_1,V_2)$, $f_1(V_1)$, and $f_2(V_2)$. When calculating those components, some assumptions are adopted by referring to existing literatures.

Table 3: Research assumptions of the critical components/parameters and their typical values pertaining to the horizontal collision risk models. DE — Double Exponential; GDE — Gaussian Double Exponential.

Component/Parameter	Related To	Assumption	Reference	Typical Value
$f_y(y)$	the expression of $P_y(S_y)$	DE Distribution	ICAO 10063, 10120	—
α	the expression of $f_y(y)$	—	ICAO 10063, 10120	$\alpha = 1 - 0.05^{1/n}$
a_2	the expression of $f_y(y)$	—	ICAO 10063, 10120	$a_2 = S_y$
$f^{AAD}(z)$	the expression of $P_z(S_z)$	DE Distribution	ICAO 9689, NLR-CR-2007-637	—
σ^{AAD}	the expression of $f^{AAD}(z)$	—	ICAO 9689, NLR-CR-2007-637	39.8 feet
$f^{ASE}(a)$	the expression of $P_z(S_z)$	GDE Distribution	ICAO 9689, NLR-CR-2007-637	—
μ_i	the expression of $f^{ASE}(a)$	—	ICAO 9689, NLR-CR-2007-637	from TSD
$\sigma_{1_i}, \sigma_{2_i}$	the expression of $f^{ASE}(a)$	—	ICAO 9689, NLR-CR-2007-637	from TSD
along-track errors	$N_{ax}(S_j)$	DE Distribution	ICAO 10063, 10120	—
cross-track errors	$N_{ax}(S_j)$	DE Distribution	ICAO 10063, 10120	—
λ	along/cross track errors	—	ICAO 10063, 10120	$-RNP/log(0.05)$
$f(V)$	$N_{ax}(S_j)$	DE Distribution	ICAO 10063, 10120	—
v_0	the expression of $f(V)$	—	ICAO 10063, 10120	480 knots
λ_v	the expression of $f(V)$	—	ICAO 10063, 10120	5.82 knots
S_x	S_x	—	ICAO 10063, 10120	120 NM

Table 3 summarizes all the assumptions of those critical components/parameters together with their typical values that have been adopted in this research by referring to official documents.

3.7. TSD Expansion Method

In order to investigate the RSM and their impact on horizontal risk with respect to future traffic demand, we develop a simple yet efficient method to expand the TSD. The developed method is presented in Algorithm 1.

Algorithm 1 Proposed method for TSD expansion for a given ATS route

Input: TSD_Org – original TSD for a given route
Output: TSD_New – new TSD for the focal route

1. TSD_New = [ ];
2. **For** ALT = 290:10:410
   a) TSD_Org1 = TSD_Org(find(TSD_Org.FL == ALT);
   b) TSD_Org1 = SortByEntryTime(TSD_Org1, 'ascend');
   c) **For** i = 1 to length(TSD_Org1)-1

i. t = TSD_Org1(i+1).EntryTime - TSD_Org1(i).EntryTime; // time difference between the entry time of two consecutive aircraft at the same FL

ii. **If** t >= 30 min

A. n_ac = floor(t/15 - 1); // number of intermediate aircraft that can be allocated

B. delta = t/(n_ac + 1); // time interval of intermediate aircraft

C. **For** j = 1 to n_ac

- TSD_cpy = TSD_Org1(i);
- TSD_cpy.FixTime = TSD_cpy.FixTime + delta*j;
- TSD_New = [TSD_New; TSD_cpy]

D. **End For**

iii. End If

d) **End For**

3. **End For**

As can be discovered from Algorithm 1, the underlying principle of the algorithm is that new traffic data will be generated between two consecutive flights from the original TSD as long as the difference between the time the two flights hit the entry fix is no smaller than 30 minutes. When interpolating the intermediate aircraft, the time duration for determining the maximum number of aircraft that can be allocated is set to be 15 minutes in a conservative way to ensure the traffic safety.

4. Experimental Settings

In order to validate the feasibility of applying RSM to procedural airspaces and analyze its corresponding impact on the collision risk, in the experimental section we will carry out a case study on the procedural airspace of Singapore FIR which has a large separation in place. This section presents the experimental settings for subsequent analysis.

4.1. Procedural Airspace of Singapore FIR

Fig. 8 visualizes the procedural airspace of Singapore FIR. As shown in the figure, there are four ATS routes which are N892, L625, N884, and M767. For Singapore FIR, the lateral and longitudinal separation minima in use for the aircraft flying in the procedural airspace are all 50 NM.

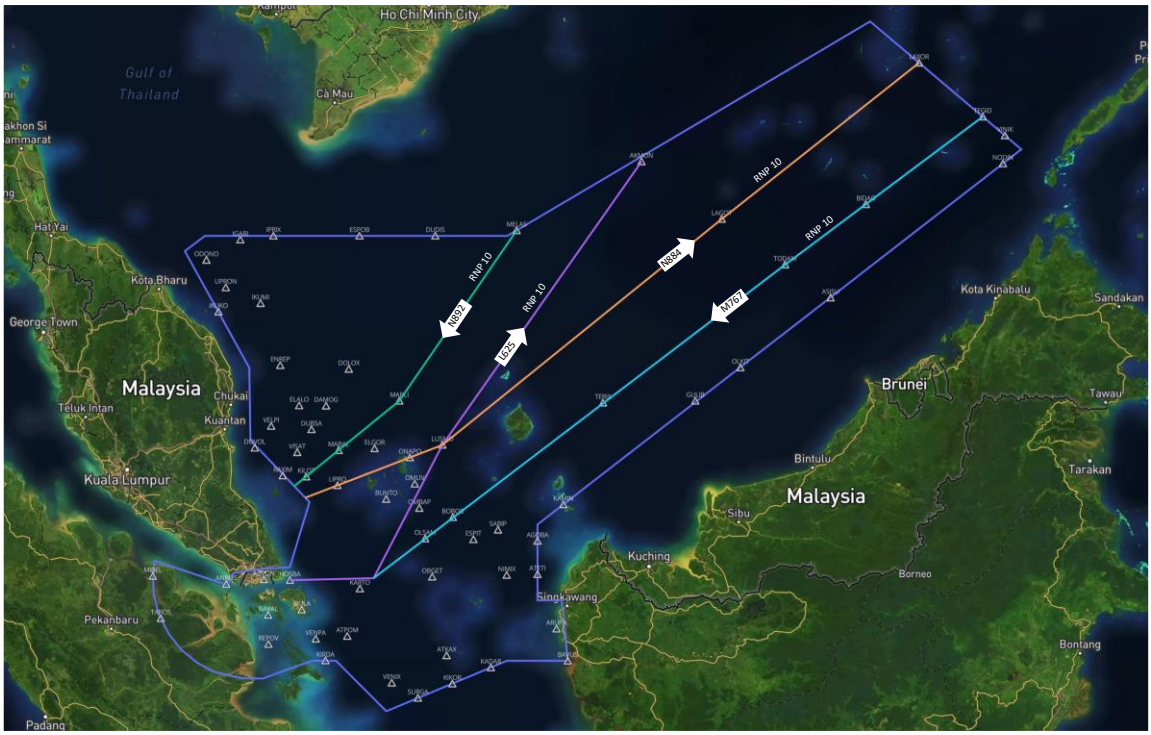

Figure 8: Visualization of the procedural airspace of Singapore FIR and the four parallel ATS routes to be studied in this work.

In Fig. 8, the arrows indicate the directions of the routes. As shown in Fig. 8, the two pairs of parallel routes are unidirectional. Note that due to the unique directions of those routes, there is only opposite-direction occupancy when calculating the lateral risk.

4.2. Traffic Sample Data

TSD is the main data that is required to estimate the collision risk. The information given in the TSD includes the date, call sign, aircraft registration number, PBN approval type, aircraft type, original aerodrome, destination aerodrome, entry fix into the airspace, time at entry fix (UTC), flight level at entry fix, route after entry fix, exit fix from airspace, time at exit fix (UTC), flight level at exit fix and route before exit fix.

The TSD used in this study is for December 2018. It records the en-route flight movements in Singapore FIR. A simplified version of the TSD containing the key information for 10 aircraft is shown in table 4. Based on the TSD, we filter out the flights on the four studied routes for subsequent analysis.

Table 4: An example of simplified TSD with 10 flights (F1-F10)

Flt	FL	Fix_1	t_1 (UTC)	Fix_2	t_2 (UTC)	Fix_3	t_3 (UTC)	Fix_4	t_4 (UTC)	Fix_5	t_5 (UTC)
F1	390	AKOMA	1/12/18 0:17	VMR	1/12/18 0:23	RAXIM	1/12/18 0:29	OTLON	1/12/18 0:30	VISAT	1/12/18 0:32
F2	360	LATHA	1/12/18 0:19	NIXUP	1/12/18 0:25	ESPOB	1/12/18 0:46	ESBUM	1/12/18 1:05	ELALO	1/12/18 1:10
F3	320	AKOMA	1/12/18 0:20	VMR	1/12/18 0:26	RAXIM	1/12/18 0:33	OTLON	1/12/18 0:33	VISAT	1/12/18 0:36
F4	350	KIMAT	1/12/18 0:25	VPK	1/12/18 0:34	BUVAL	1/12/18 0:37	VEPLI	1/12/18 0:41	NOPAT	1/12/18 0:48
F5	300	ATETI	1/12/18 0:29	NIMIX	1/12/18 0:33	OBGET	1/12/18 0:42	TOMAN	1/12/18 0:49		
F6	360	KIMAT	1/12/18 0:29	VPK	1/12/18 0:40	BUVAL	1/12/18 0:42	VEPLI	1/12/18 0:46	NOPAT	1/12/18 0:52
F7	350	AKOMA	1/12/18 0:29	VMR	1/12/18 0:36	RAXIM	1/12/18 0:43	OTLON	1/12/18 0:44	VISAT	1/12/18 0:47
F8	400	HOSBA	1/12/18 0:32	TOMAN	1/12/18 0:46	VERIN	1/12/18 0:57	LUSMO	1/12/18 1:06	AKMON	1/12/18 1:49
F9	330	KIMAT	1/12/18 0:35	VPK	1/12/18 0:45	IDSEL	1/12/18 0:50	URIGO	1/12/18 0:51	VISAT	1/12/18 0:55
F10	390	AKOMA	1/12/18 0:37	VMR	1/12/18 0:44	RAXIM	1/12/18 0:50	OTLON	1/12/18 0:51		

4.3. Data Pre-processing

In order to facilitate the collision risk estimation process, data pre-processing process is needed to clean the original TSD due to the noise contained in the data. Specifically, the following criteria are adopted to remove flights from the TSD.

1) Flights that do not have valid aircraft dimensions (each aircraft will be retrieved from a database containing the dimension information for diverse kinds of aircraft).

2) Flights that only carry with one waypoint information.

3) Flights that do not have any waypoints within Singapore FIR.

4) Flights that have no flight path information.

5) Flights that have zero travel time (for some flights, it has been found that the travelling time durations between two consecutive waypoints are zero due to anthropogenic errors).

6) Flights that have abnormal ground speed (in the analysis, as long as the ground speed of a flight on an airway segment is outside of the range [210, 600] knots, then the flight is removed from the TSD).

For the studied TSD, there are a total of 44,215 flights. After the cleaning process based upon the above criteria, 33,366 flights are kept for subsequent collision risk estimation. It should be pointed out that although around 25% of the flights have been removed, those flights have little impact on the collision risk calculation. For one thing, the majority of the removed flights are flights outside Singapore airspace. Those flights contribute nil to the collision risk calculation for Singapore FIR. For another thing, the remaining flights that have been removed are mainly flights without dimension information (flights that cannot be retrieved from the flight database) and abnormal flights (zero flight time and abnormal ground speed). These flights are unsuitable for collision risk calculation.

4.4 Parameter Settings

Based on those assumptions listed in Table 3, we further work out the values of other components/parameters that relay on those assumptions. Table 5 records the values of the key parameters involved in the horizontal collision risk models.

Table 5: Values of the key parameters involved in the horizontal collision risk models. Most of the values are derived from the cleaned one-month TSD for Singapore FIR

Lateral risk (Eq. 1)		Longitudinal risk (Eq. 4)		New Intervention
Parameters	Values	Parameters	Values	Mode (Eq. 5)
λ_x	0.02605 NM	λ_{xy}	0.02605 NM	/
λ_y	0.02356 NM	λ_z	0.00744 NM	/
λ_z	0.00744 NM	λ_v	5.82 knots	6.5 knots
S_y	50 NM	S_x	50 NM	/
S_X	120 NM	V_1	460.367 knots	/
$\overline{V}$	460.37 knots	V_2	460.367 knots	/
$P_z(0)$	0.538	$P_z(h_z)$	0.568	/
$P_y(S_y)$	1.75×10^{-8}	T	27 min	3.2 min
$E_y(same)$	0	NP	1	4
$E_y(opp)$	0.125	$D_x(t)$	—	/
$\lvert\overline{\dot{y}(S_y)}\rvert$	75 knots	τ	[4, 10.5, 13.5] min	/
$\lvert\overline{\dot{z}}\rvert$	1.5 knots	$\lvert\overline{\dot{z}}\rvert$	1 knots	1.5 knots

As can be seen from Table 5, parameters of S_x and S_y are set to be constants as they are the planned separation minima. For parameters such as $P_z(0)$, $\lvert\overline{\dot{y}(S_y)}\rvert$, and $\lvert\overline{\dot{z}}\rvert$, they are also set to be constants. This setting is line with what other airspaces are doing. For parameters such as λ_x, λ_y, λ_z, $P_y(S_y)$, and $\overline{V}$, they are estimated based on the TSD as they are dependent on the specific traffic scenario.

5. Impact of RSM on Collision Risk

This section demonstrates the case study on the procedural airspace of Singapore FIR with respect to reduced horizontal separation minima. The collision risk with respect to current separation minima and new separation minima will be analyzed based on one-month traffic data provided by the Civil Aviation Authority of Singapore (CAAS).

5.1. RSM and Lateral Risk with Current Demand

For Singapore FIR, the lateral separation minimum in use for the aircraft flying in the procedural airspace is 50 NM. In order to investigate how the lateral separation minimum affect the lateral collision risk, a wide range of [20, 50] NM for the lateral separation minimum is set.

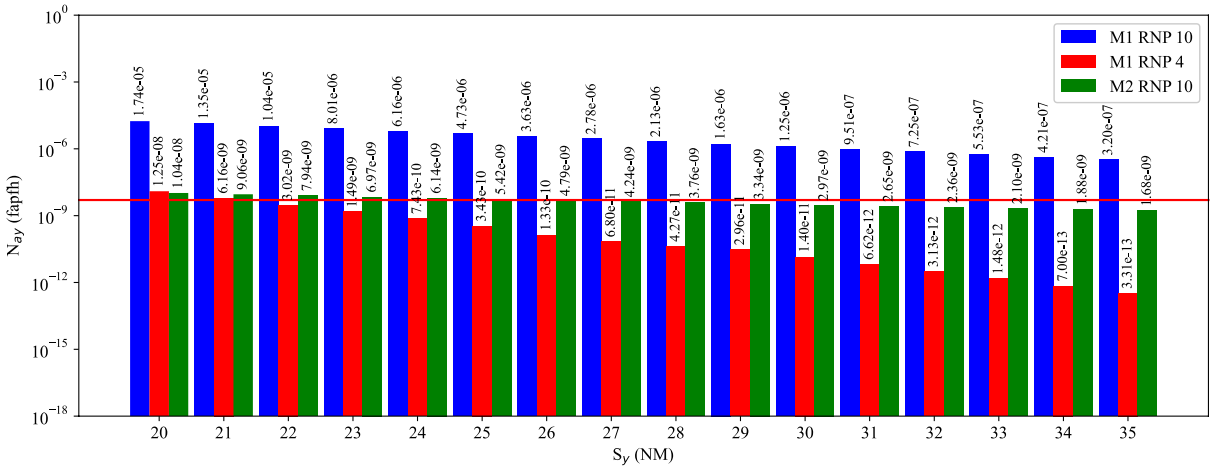

(a) *Nay with respect to* S_y ($S_y \in Z | 20 \leq S_y \leq 35$)

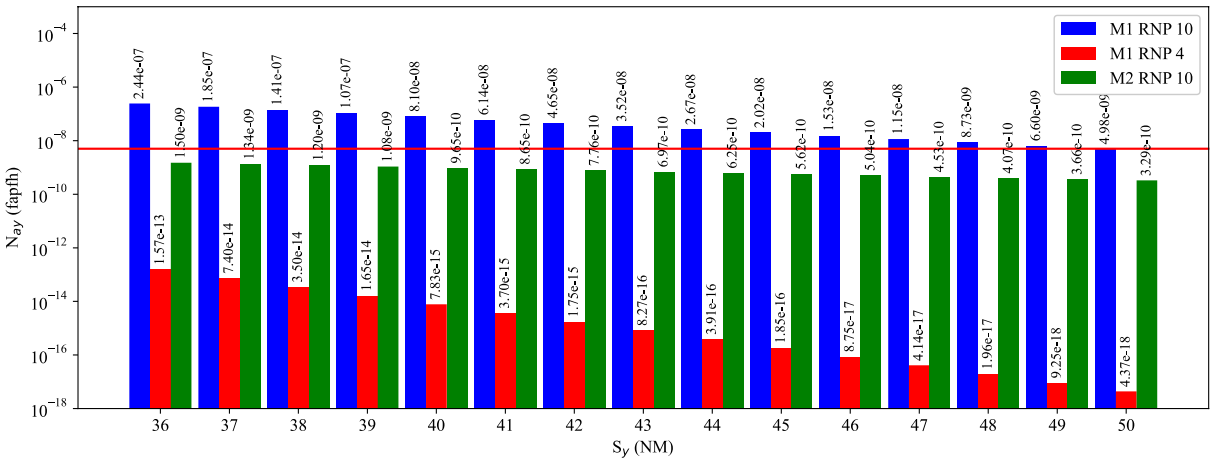

(b) *Nay with respect to* S_y ($S_y \in Z | 36 \leq S_y \leq 50$)

Figure 9: Lateral risk with respect to different separation standards of (a) $S_y \in Z | 20 \leq S_y \leq 35$ *and (b)* $S_y \in Z | 36 \leq S_y \leq 50$ *when applied to the procedural airspace of Singapore FIR.*

Regarding the lateral collision risk, there are two types of occupancy, namely same direction occupancy and opposite direction. However, the two pairs of parallel routes in the procedural airspace of Singapore FIR, as shown in Fig. 8, are in opposite direction. So only the opposite occupancy is required to be computed.

Figs. 9a and 9b demonstrate the comparisons of the lateral collision risk with respect to different lateral separation standards and RNP specifications. It can be clearly seen from Fig. 9b that the lateral risk is quite close to the TLS with current procedures ($S_y = 50$ NM, RNP10) when model M1 is considered for calculating the lateral overlap probability. Model M2 can lead to smaller lateral risk, as can be seen from Fig. 9. Fig. 9b also shows that the lateral risk with respect to model M1 exceeds the TLS if S_y decreases, which indicates that the lateral separation cannot be further reduced with current procedures.

With advanced CNS technologies, RNP 4 can be applied to the en-route airspace. Figs. 9a and 9b clearly show that the lateral collision risk can be further reduced with RNP 4. The lateral risk will surpass the TLS if the lateral separation minimum is smaller than 22 NM. The above analysis indicates that, if RNP 4 is to be implemented, then the lateral separation minimum can be within the range of [22, 50] NM with respect to the current traffic scenario.

5.2. RSM and Longitudinal Risk with Current Demand

For the longitudinal separation minimum, a range of [20, 50] NM has also been set to explore the promising range of RSM in the longitudinal plane. In order to estimate the longitudinal risk, it is needed to figure out the distribution of the longitudinal separation.

5.2.1. Distributions of the Longitudinal Separation

Figs. 6 and 7 show how to derive the separations from a given TSD. Based on the derived separations, curve fitting technique is introduced to estimate the distribution of the longitudinal separations. In this study, four distributions, i.e., Gamma (GMA), Log-normal (LGN), Normal (NML) and Weibull (WBL), are introduced, and below are their probability density functions.

$$GMA: f(x) = \frac{1}{\Gamma(k)\theta^k} x^{k-1} e^{-\frac{x}{\theta}} \tag{7}$$

$$LGN: f(x) = \frac{1}{x\sigma\sqrt{2\pi}} e^{-\frac{(\ln x - \mu)^2}{2\sigma^2}} \tag{8}$$

$$NML: f(x) = \frac{1}{\sigma\sqrt{2\pi}} e^{-\frac{1}{2}\left(\frac{x-\mu}{\sigma}\right)^2} \tag{9}$$

$$WBL: f(x) = \frac{1}{\lambda}\left(\frac{x}{\lambda}\right)^{k-1} e^{-\left(\frac{x}{\lambda}\right)^{k}} \qquad (10)$$

Note that the definitions and meanings of the parameters involved in the above shown equations are not provided because they are well-known and it is assumed that readers are familiar with those probability density functions.

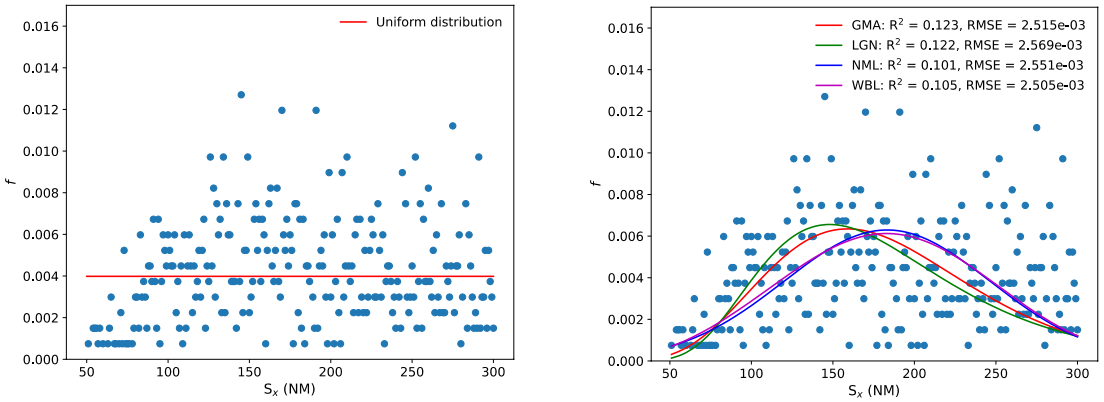

(a) *Case 1* (b) *Case 2*

Figure 10: Distribution of longitudinal separations derived from TSD with respect to case 1 and case 2 and the corresponding curve fittings.

The initial inter-pair longitudinal separation distribution derived from the Singapore TSD with respect to case 2 is presented in Fig. 10 together with the curve fitting results. Fig. 10 shows that the log-normal distribution has the best fit as it has the highest R^2 value and lowest RMSE as compared to other distributions.

It should be noted that the distribution of the separation derived from the TSD with respect to case 2 does not seem to follow any distribution, as the R^2 values as shown in Fig. 10 are quite small. Since the R^2 value with respect to the Gamma distribution is largest amongst the three density functions, in the subsequent analysis we take it that the longitudinal separation distribution follows the Gamma distribution. In what follows the distribution with respect to case 3 will be analyzed.

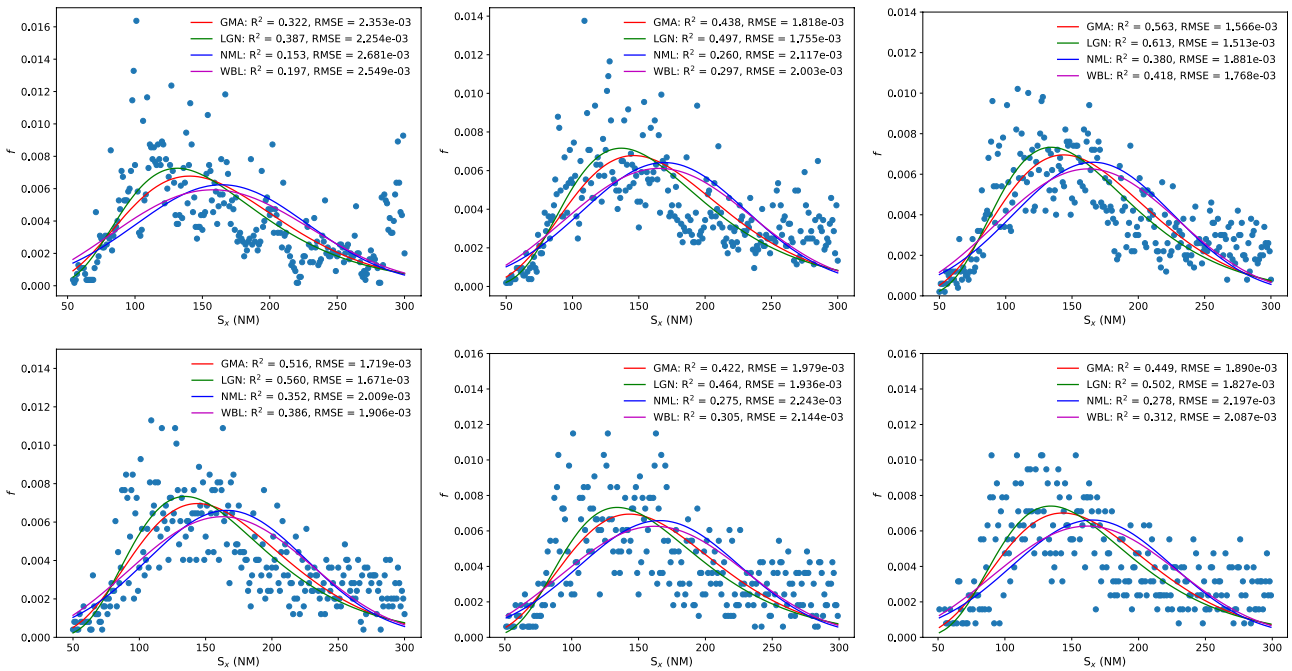

Figure 11: Distributions of longitudinal separations derived from TSD with respect to case 3 under different time intervals (1 min, 3 min, 5 min, 10 min, 15 min, 20 min) and the corresponding curve fittings.

Fig. 11 demonstrates the distributions of longitudinal separations with respect to case 3 under different time intervals. The curve fitting results indicate that the distribution of the longitudinal separations follows the log-normal distribution with respect to case 3. The parameters involved in the log-normal distribution with respect to different time intervals are:

1) $\delta = 1\,min, \sigma = 0.38818, \mu = 5.02800$;
2) $\delta = 3\,min, \sigma = 0.37930, \mu = 5.06172$;
3) $\delta = 5\,min, \sigma = 0.37720, \mu = 5.04284$;
4) $\delta = 10\,min, \sigma = 0.37650, \mu = 5.04388$;
5) $\delta = 15\,min, \sigma = 0.37831, \mu = 5.04120$;
6) $\delta = 20\,min, \sigma = 0.37439, \mu = 5.03975$.

5.2.2. Longitudinal Risk Under the Three Cases

Based on the three cases, the longitudinal risk is calculated with respect to different S_x and intervention models shown in Fig. 4 and Fig. 5. Fig. 12 presents the estimated longitudinal risk under case 1, case 2, and case 3. Note that RNP 10 is considered in Fig. 12a while RNP 4 is considered in Fig. 12b.

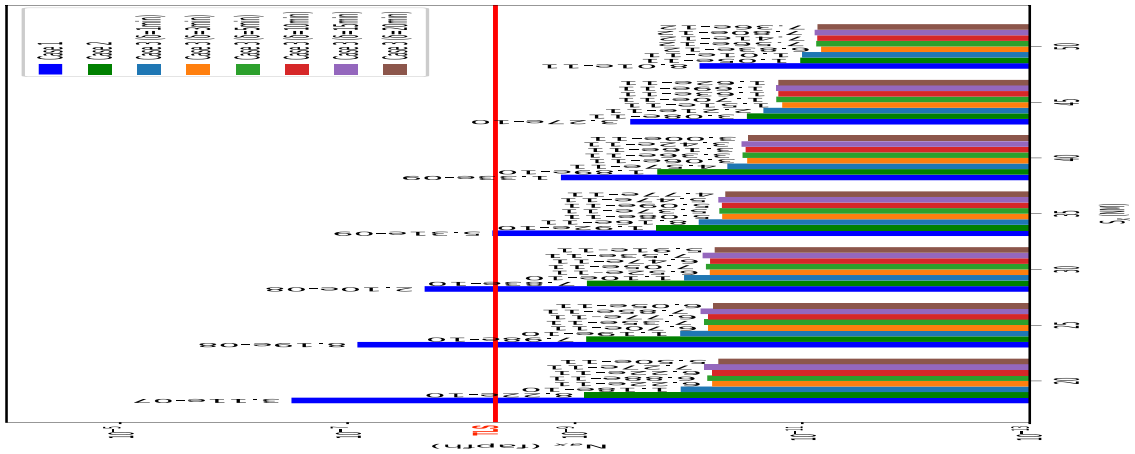

(a) *Current Intervention Model*

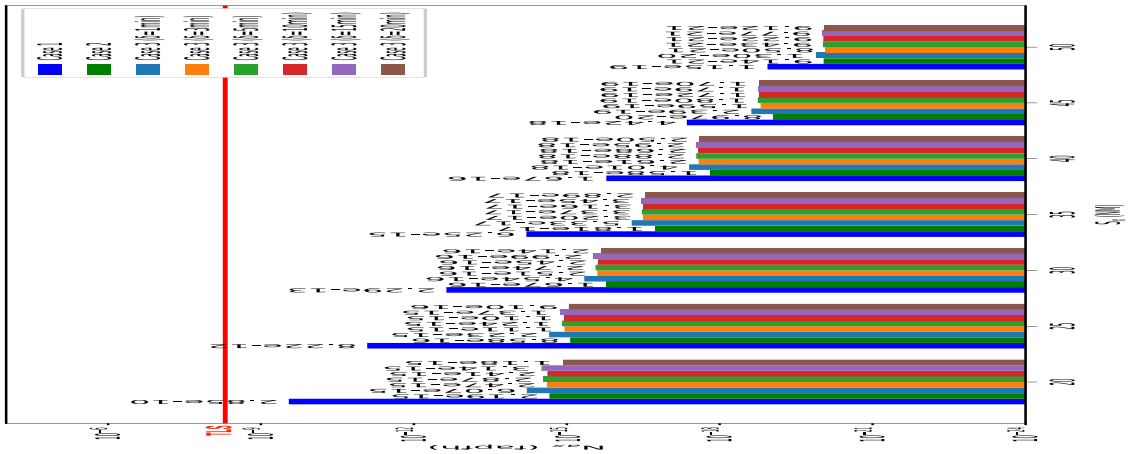

(b) *New Intervention Model*

Figure 12: Longitudinal risk under case 1, case 2 and case 3 with respect to different separation standards and intervention models.

Case 1 is very conservative. This is why the corresponding risk recorded in Fig. 12 are higher than those with respect to case 2. The results shown in Fig. 12 indicate that the longitudinal risk under current control procedures are below the TLS under cases 1 and 2. Fig. 12a suggests that the longitudinal separation can be reduced to 35 NM given the current control procedures, while Fig. 12b indicates that a further reduced separation of 20 NM can be implemented with advanced CNS.

For case 3, it is obvious from Fig. 12 that the collision risk with respect to case 3 is below the TLS with current control procedures. When new CNS technologies are employed, then the longitudinal separation for the procedural airspace of Singapore FIR can be reduced to 20 NM under case 3, while the collision risk still can meet the TLS.

As can be seen from the above experiments, advanced CNS technologies both affect the RSM and the corresponding collision risk. Advanced communication techniques, such as improved CPDLC services, can help controllers reduce the intervention time for conflict resolution. Improved navigation specifications such as RNP 4 can reduce aircraft lateral deviation frequencies, while better surveillance services such as space-based ADS-B, can reduce horizontal overlap probabilities. Regarding the horizontal collision risk, advanced CNS technologies affect the values of components, such as $P_y(S_y)$, S_y, S_x, etc., involved in the collision risk models. A minima lateral/longitudinal separation therefore can be derived by setting the upper limit of the resultant collision risk to be the TLS.

5.3. Future Demand Simulation

The above section investigates the impact of RSM on horizontal risk with respect to current traffic demand. Intuitively, if the separation minima are reduced, then the traffic demand can be increased. The following sections aim to investigate the impact of RSM on the horizontal risk with respect to future traffic demand.

5.3.1. Data-Driven Demand Analysis

In order to investigate the impact of RSM on the horizontal risk under future demand, the first thing that we need to do is to generate new TSD that can simulate future demand based on current TSD. To do so, we first present a holistic view of current demand with respect to the available TSD. A data-driven method for deriving the traffic demand from the TSD is therefore developed.

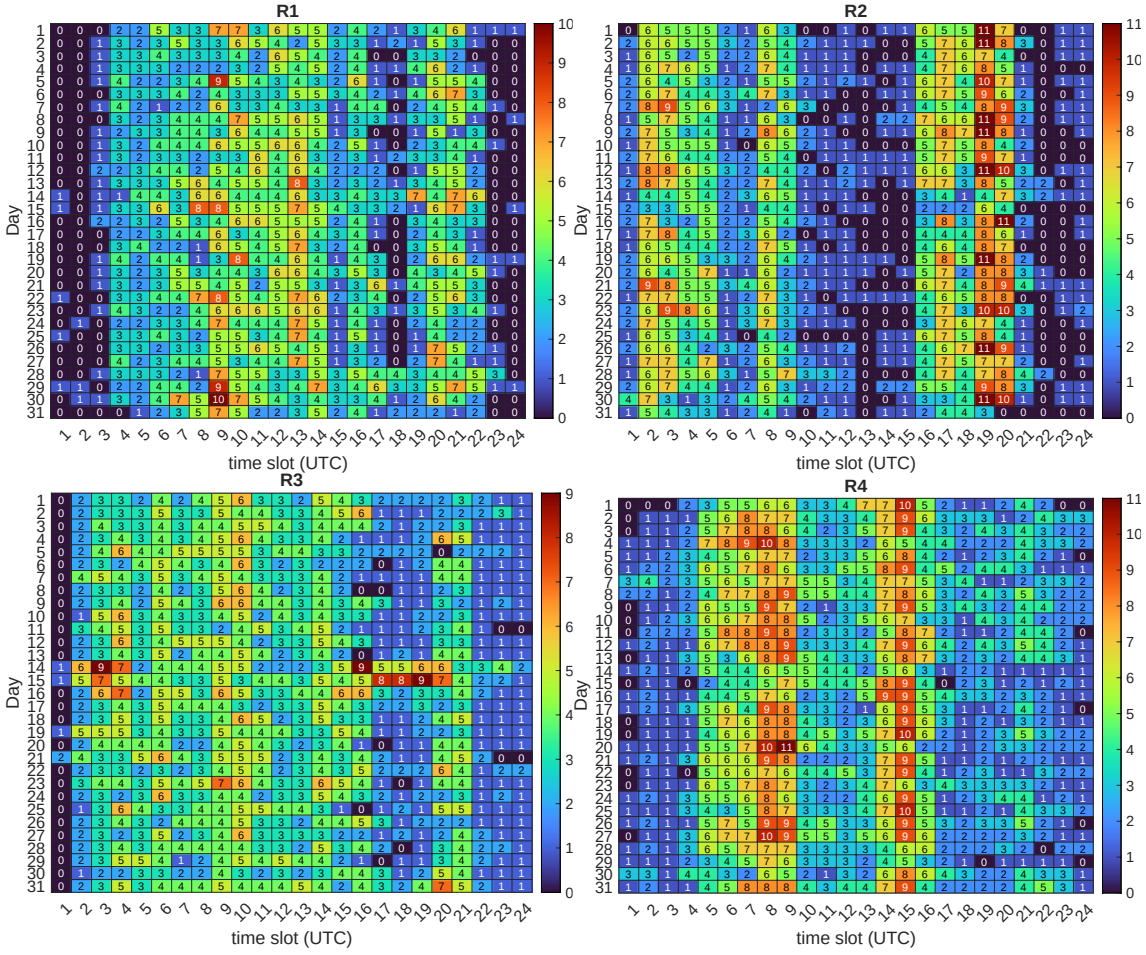

Figure 13: Hourly demands on the four routes derived from the one-month TSD. The starting time point is 00:00 am UTC.

For the studied procedural airspace, there are four routes, viz., N892, L625, N884, and M767. Hereafter, we represent them by R1, R2, R3, and R4, respectively, for simplicity. For a given route, say R1, we first filter out all the flights that pass through R1 from the one-month TSD. We then sort all the filtered flights in an ascending order based on the first time points pertaining to the flights' flying profile. Finally, we count the number of flights passing through route R1 per hour. We set the starting time point to be 00:00 UTC. The average flight rate over 31 days (because the TSD is for every December) is then taken as the demand on the studied route.

Based on the one-month TSD, we obtain the demands of the four studies routes using the method described above. Fig. 13 shows the corresponding results. As can be seen from Fig. 13, the hourly demands on the four routes vary a lot. Route R4 and route R1 are the busiest routes as they serve 28.81% and 27.19% of the traffic, respectively, while routes R2 and R3 accommodate 25.82% and 18.18% of the traffic, respectively. Based on Fig. 13, we get the average demands on R1, R2, R3 and R4, which are $D_{R_1} = 2.85\ ac/hr$, $D_{R_2} = 3.10\ ac/hr$, $D_{R_3} = 2.93\ ac/hr$, $D_{R_4} = 3.66$ ac/hr, respectively.

5.3.2. Expanded TSD

Fig. 13 clearly shows that the average demands on the four studied routes are quite below their peaks. This indicates that there is large space to expand the TSD to simulate the future traffic demand. This is the main reason why we develop Algorithm 1 to expand the TSD.

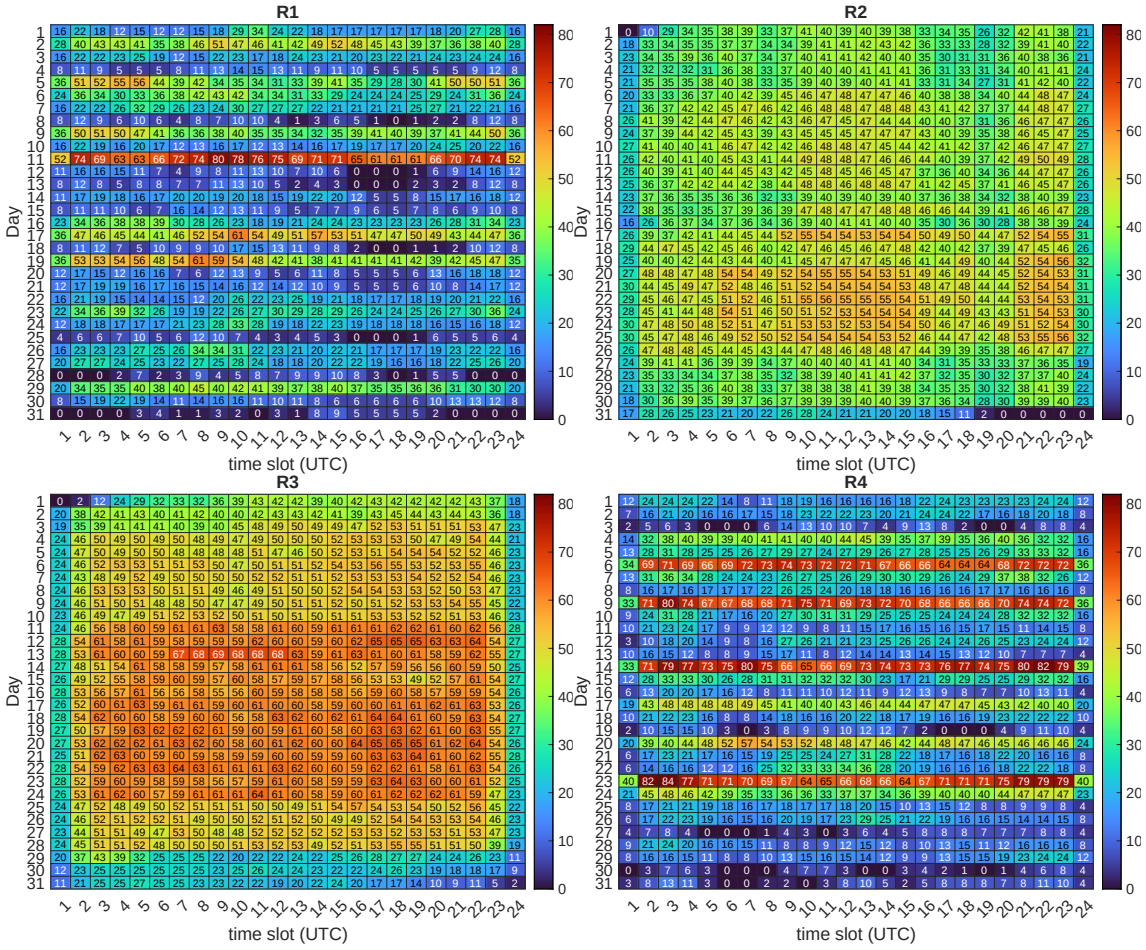

Figure 14: Hourly demands on the four routes derived from the four expanded TSD, i.e., TSD_R1, TSD_R2, TSD_R3, and TSD_R4.

Note that Algorithm 1 is for a single route. We apply Algorithm 1 to each of the four studied routes and therefore obtain four expanded TSD denoted by TSD_R1, TSD_R2, TSD_R3, and TSD_R4. Fig. 14 shows the hourly demands on the four routes based on the expanded TSD using the data-driven demand analysis method presented above. As compared to Fig. 13, the expanded TSD have hourly demands which are roughly 9x of the original demands. Based on Fig. 14, we get the average demands on R1, R2, R3 and R4, which are $D_{R_1} = 21.92\ ac/hr, D_{R_2} = 40.11\ ac/hr, D_{R_3} = 48.66\ ac/hr, D_{R_4} =$

25.70 ac/hr, respectively. Note that the demands shown in Fig. 13 and Fig. 14 are for all the 13 flight levels from FL290 to FL410. Therefore, an hourly demand of 80 aircraft on a single route is feasible.

We can clearly observe from Figs. 13 and 14 that the newly obtained TSD have more flights than the original TSD does. This phenomenon is mainly due to the fact that we observe from the original TSD that there is no flight (zero values as shown in Fig. 13) on each of the routes for certain time periods. We further observe that those time periods are as long as several days, as can be seen from Fig. 13. As a consequence, Algorithm 1 will generate the flying profiles for a large amount of flights during those periods.

5.4. RSM and Lateral Risk with Future Demand

As can be inferred from Fig. 14, the expanded TSD have much higher demands than the original TSD. Recall the results presented in Fig. 9 which indicate that S_y can be reduced to 24 NM with current demand under RNP 4. In this section, we would like to see the minima S_y with respect to increased demands.

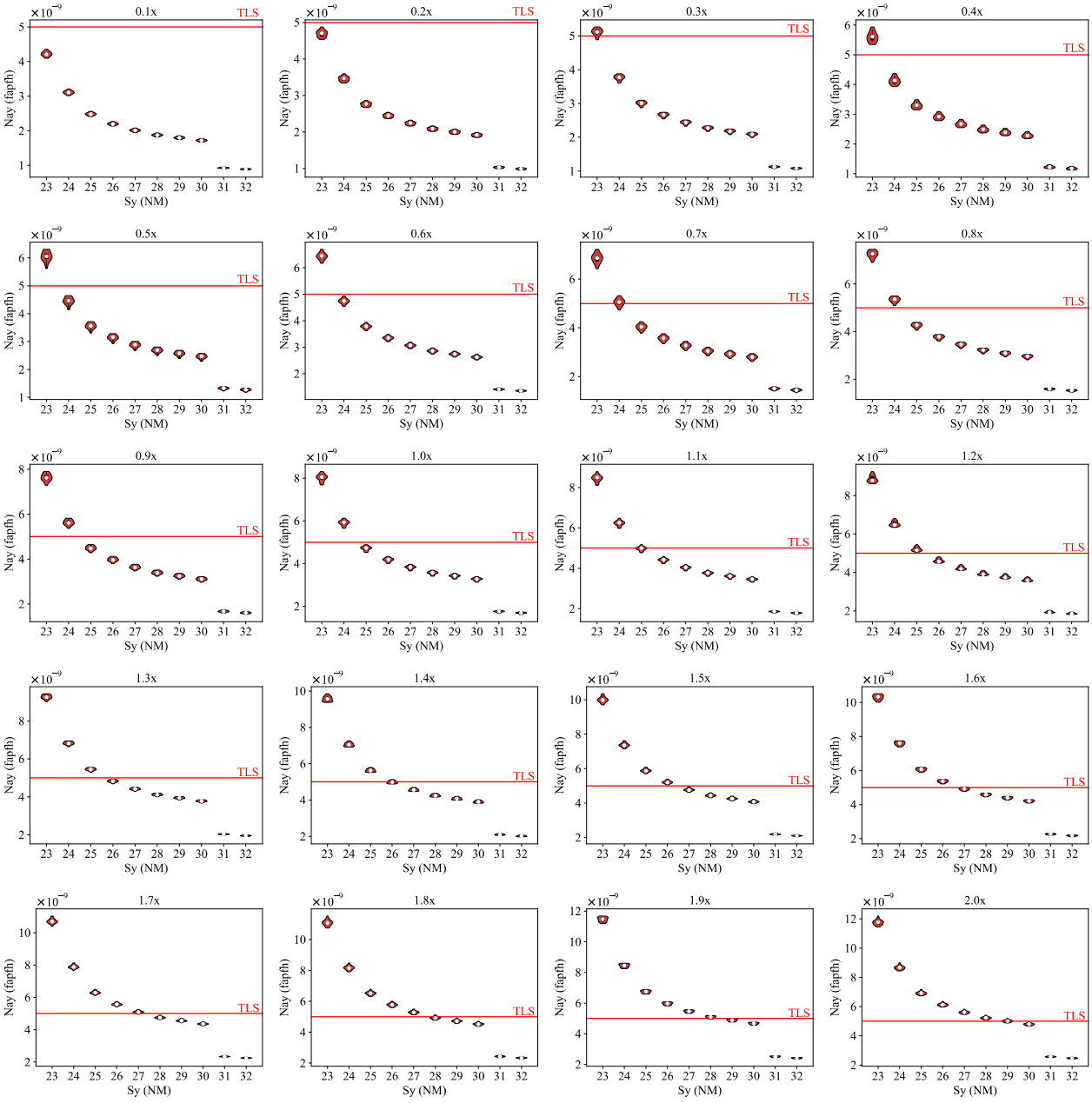

Figure 15: Lateral risk with respect to varying separation standards S_y and different portions (10%~200% at an interval of 10%) of increased traffic demands when applied to the procedural airspace of Singapore FIR.

From the original TSD, we can get to know the original demands on the four routes, say $D^0_{R_1}, D^0_{R_2}, D^0_{R_3}$ and $D^0_{R_4}$. Then we increase the demands for the four routes by a given portion, say $p\%$. In

order to estimate the lateral risk, we randomly sample $D^0_{R_1} \times p\%$, $D^0_{R_2} \times p\%$, $D^0_{R_3} \times p\%$, and $D^0_{R_4} \times p\%$ flights from TSD_R1, TSD_R2, TSD_R3, and TSD_R4, respectively. Then we merge the four sampled TSD with the original TSD, forming a new one-month TSD. Afterward, we calculate Nay using the new TSD.

Fig. 15 visualizes the distributions of N_{ay} with respect to varying S_y and $p\%$. For a given value of p, we do the TSD sampling for 50 times since the expanded TSD are quite large in size. We can see from Fig. 15 that when the demand is increased by 0.2x, the minimum S_y becomes 23 NM, while the Nay still meets the TLS standard. Fig. 15 also shows that if the demand is doubled (1.0x), then S_y can be reduced from 50 NM to 25 NM. Fig. 15 further indicates that when we increase the demand by 2.0x, the minimum S_y can be reduced to 31 NM.

The results recorded in Fig. 15 are quite valuable to ANSPs. Fig. 15 provides scientific insights for ANSPs to understand the relationship between increased traffic demands and the resultant lateral risk, thereby assisting network managers with their decision makings for airspace and/or traffic management.

5.5. RSM and Longitudinal Risk with Future Demand

The above section investigates the lateral collision risk under future demand. This section therefore investigates the longitudinal risk under future demand with respect to different longitudinal separations. Note that the calculation of N_{ax} is time consuming. During the analysis, we therefore only consider case 1 as discussed in subsection 3.5.1. Case 1 is a conservative way for estimating the longitudinal risk.

Table 6: Longitudinal risk with respect to varying separation standards S_x and different portions (20%~180% at an interval of 20%) of increased traffic demands when applied to the procedural airspace of Singapore FIR.

Model	$p\%$	$S_x = 20\ NM$	$S_x = 25\ NM$	$S_x = 30\ NM$	$S_x = 35\ NM$	$S_x = 40\ NM$	$S_x = 45\ NM$	$S_x = 50\ NM$
old model	0.2x	2.2169e-06	7.6331e-07	2.5248e-07	8.1107e-08	2.5502e-08	7.8927e-09	2.4142e-09
	0.4x	2.2469e-06	7.7345e-07	2.5578e-07	8.2154e-08	2.5827e-08	7.9923e-09	2.4444e-09
	0.6x	2.2615e-06	7.7858e-07	2.5751e-07	8.2714e-08	2.6005e-08	8.0478e-09	2.4615e-09
	0.8x	2.2815e-06	7.8535e-07	2.5971e-07	8.3412e-08	2.6222e-08	8.1145e-09	2.4817e-09
	1.0x	2.2961e-06	7.9047e-07	2.6143e-07	8.3972e-08	2.6400e-08	8.1701e-09	2.4988e-09
	1.2x	2.3061e-06	7.9385e-07	2.6253e-07	8.4321e-08	2.6509e-08	8.2033e-09	2.5089e-09
	1.4x	2.3262e-06	8.0063e-07	2.6474e-07	8.5021e-08	2.6726e-08	8.2699e-09	2.5291e-09
	1.6x	2.3362e-06	8.0403e-07	2.6584e-07	8.5371e-08	2.6835e-08	8.3033e-09	2.5392e-09
	1.8x	2.3408e-06	8.0575e-07	2.6646e-07	8.5580e-08	2.6904e-08	8.3254e-09	2.5462e-09
	2.0x	2.3608e-06	8.1253e-07	2.6867e-07	8.6280e-08	2.7121e-08	8.3920e-09	2.5664e-09
new model	0.2x	1.5109e-09	5.6521e-11	2.1973e-12	8.6193e-14	3.4504e-15	1.3073e-16	4.3771e-18
	0.4x	1.5312e-09	5.7261e-11	2.2256e-12	8.7277e-14	3.4930e-15	1.3232e-16	4.4301e-18
	0.6x	1.5412e-09	5.7646e-11	2.2408e-12	8.7886e-14	3.5178e-15	1.3327e-16	4.4621e-18
	0.8x	1.5547e-09	5.8139e-11	2.2597e-12	8.8609e-14	3.5462e-15	1.3433e-16	4.4974e-18
	1.0x	1.5648e-09	5.8524e-11	2.2749e-12	8.9219e-14	3.5710e-15	1.3528e-16	4.5294e-18
	1.2x	1.5715e-09	5.8771e-11	2.2843e-12	8.9580e-14	3.5851e-15	1.3581e-16	4.5471e-18
	1.4x	1.5851e-09	5.9265e-11	2.3032e-12	9.0304e-14	3.6136e-15	1.3687e-16	4.5824e-18
	1.6x	1.5918e-09	5.9512e-11	2.3126e-12	9.0666e-14	3.6278e-15	1.3741e-16	4.6001e-18
	1.8x	1.5951e-09	5.9649e-11	2.3184e-12	9.0913e-14	3.6383e-15	1.3782e-16	4.6144e-18
	2.0x	1.6086e-09	6.0144e-11	2.3373e-12	9.1636e-14	3.6668e-15	1.3889e-16	4.6498e-18

As presented in section 3, the longitudinal risk calculation is related to the specific controller intervention model. The results demonstrated in Fig. 12a indicate that the longitudinal separation S_x can be reduced to from 50 NM to 36 NM with respect to current demand and intervention model when a

uniform distribution of S_x is assumed. As shown in Fig. 12b, if new intervention model is adopted, then S_x can be reduced to 20 NM under current demand while N_{ax} is still below the TLS. In view of this, we analyze the longitudinal risk under future demands with respect to the two intervention models. The corresponding results are recorded in Table 6.

Table 6 clearly shows that when p increases, the longitudinal risk also increases. However, the increment of N_{ax} is quite small. When the current intervention model is considered, the traffic demand can be increased by 2.0x without the need to alter the longitudinal separation minimum. The results shown in the last column of the table even suggest that the longitudinal separation can be slightly reduced (larger than 45 NM) as N_{ax} is small than the TLS. When the new intervention model is considered, then we can observe from Table 6 that N_{ax} has been largely decreased. Even though we increase the demand by 2.0x, the longitudinal separation still can be reduced to 20 NM, while the risk is about 1.6×10^{-9} fapfh.

6. Concluding Remarks

Air transport is an indispensable part of the domestic as well as the international transportation systems due to its significant contribution to the economics. With the projected increase in demand for both passengers and air cargo in a post-COVID-19 scenario, airspace may encounter unprecedented traffic movements. In order to maintain safety of air traffic operations, stringent air traffic separation standards are in place where aircraft are separated vertically and horizontally based on certain separation minima to avoid mid-air collision.

Note that the separation minima for aircraft flying in a procedural airspace covered by limited CNS services are normally larger than those for a non-procedural airspace. With the advancement of CNS technologies for air traffic such as space-based ADS-B, large separation minima may be reduced and can significantly contribute to counterbalance the imbalance between the limited airspace capacity and increasing air traffic demand. The reduction on separation minima will affect the collision risk of the traffic within a given volume of airspace. It is of great significance to ANSPs to explore the extent to which the reduced separation minima can be achieved while still maintaining the acceptable level of traffic collision risk.

This paper aims to investigate the feasibility of reduced horizontal separation minima to a procedural airspace and the corresponding impact on traffic collision risk. To do so, this paper first presented the CREAM software developed by the authors. The CREAM software exempts aviation decision makers from the complicated collision risk models by providing a user-friendly collision risk estimation interface. Meanwhile, the CREAM software is able to estimate collision risk at fine grained levels, i.e., waypoints and airway segments, which provides visual clues regarding collision risk for decision makers. Then this paper presented the adoptions of the horizontal collision risk models with respect to advanced CNS techniques. At last, this paper carried out a case study on the procedural airspace of Singapore FIR in which the lateral and longitudinal separation standards are both 50 NM. The horizontal risk with respect to a one-month TSD had been analyzed with respect to different control procedures (different separation minima, different CNS specifications, and different traffic scenarios). The results indicated that, with current control procedures, the lateral and longitudinal collision risk all meet the TLS standards. The results further indicated that, if RNP 4 is implemented to the Singapore procedural airspace, then the current lateral and longitudinal separation minima can be reduced from 50 NM to 22 NM and 20 NM, respectively, while the corresponding collision risk still meets the TLS standards.

Note that the traffic demand is envisaged to increase in the future. It would be very helpful if the collision risk with respect to future demands also can be estimated. In view of this, the paper developed a simple algorithm to expand the existing traffic data to simulate future traffic demands. The horizontal risk with respect to increased traffic demands were analyzed. A parameter $p\%$ was introduced to control the increment of the traffic demand. The horizontal risk with respect to p varying from 10 to 200 were estimated and the corresponding minimum separation standards were identified. It was discovered that when the demand was increased by 2.0x, the lateral and longitudinal separations could be reduced to 31 NM and 20 NM respectively, while the corresponding risk were still below the TLS.

Note that the research findings revealed in this study are based upon certain assumptions. Regarding the collision risk estimation, many assumptions like the double exponential distributions as mentioned in the simulation section are adopted in order to estimate the collision risk. One may also try to adopt

other assumptions or even pure data-driven methods to estimate the key components and parameters involved in the collision risk models. As a consequence, the final horizontal risk could slightly differ from what are reported in this study and the feasible separation minima could also vary.

Acknowledgement

The authors would like to thank Civil Aviation Authority of Singapore (CAAS) POCs for their useful discussions and feedback. This research is supported by the National Research Foundation, Singapore, and the CAAS, under the Aviation Transformation Programme. Any opinions, findings and conclusions or recommendations expressed in this material are those of the author(s) and do not reflect the views of National Research Foundation, Singapore and the CAAS.

References

[1] European Commission, SESAR project. URL https://ec.europa.eu/transport/modes/air/sesar_en

[2] K. Button, R. Neiva, Single European sky and the functional airspace blocks: Will they improve economic efficiency?, Journal of Air Transport Management 33 (2013) 73–80.

[3] SESAR Joint Undertaking, A proposal for the future architecture of the European airspace (2019). URL https://www.sesarju.eu/sites/default/files/documents/reports/Future%20Airspace%20Archi tecture%20Proposal.pdf

[4] FAA, NextGen-SESAR, state of harmonisation. 2nd Edition (2016).

[5] SESAR JU, NextGen-SESAR, state of harmonisation. 3rd edition (2018).

[6] M. M. Hossain, A. Sameer, D. Delahaye, An evolutionary computational framework for capacity-safety trade-off in an air transportation network, Chinese Journal of Aeronautics 32 (4) (2019) 999–1010.

[7] Y. Wang, M. Li, K. Gopalakrishnan, T. Liu, Timescales of delay propagation in airport networks, Transportation Research Part E: Logistics and Transportation Review, 161 (2022) 102687.

[8] Y. Wang, J. Zhan, X. Xu, L. Li, P. Chen, M. Hansen, Measuring the resilience of an airport network, Chinese Journal of Aeronautics 32 (12) (2019) 2694-2705.

[9] W. Du, M. Zhang, Y. Zhang, X. Cao, J. Zhang, Delay causality network in air transport systems, Transportation Research Part E: Logistics and Transportation Review, 118 (2018) 466-476.

[10] X. Guan, R. Lyu, H. Shi, J. Chen, A survey of safety separation management and collision avoidance approaches of civil UAS operating in integration national airspace system, Chinese Journal of Aeronautics 33 (11) (2020) 2851–2863.

[11] C. Ma, Q. Cai, S. Alam, B. Sridhar, V. Duong, Airway network management using Braess's paradox, Transportation Research Part C: Emerging Technologies 105 (2019) 565–579.

[12] FAA, Certification considerations associated with the proposal to expand the upper limit of RVSM airspace, https://www.faa.gov/air_traffic/separation_standards/rvsm/documents/ASE/3.3_Upper_Limit_RVSM_Airspace.pdf.

[13] W. Du, X. Zhou, O. Lordan, Z. Wang, C. Zhao, Y. Zhu, Analysis of the Chinese Airline Network as multi-layer networks, Transportation Research Part E: Logistics and Transportation Review 89 (2016) 108-116.

[14] ICAO, Manual on Implementation of a 300 m (1000 ft) Vertical Separation Minimum Between FL 290 and FL 410 Inclusive (Doc 9574, AN/934), 2nd Edition (2002).

[15] S. Silva, A brief history of RVSM, https://www.icao.int/esaf/documents/rvsm/2010/afi%20riss/presentations.pdf.

[16] S. Alam, C. Lokan, G. Aldis, S. Barry, R. Butcher, H. Abbass, Systemic identification of airspace collision risk tipping points using an evolutionary multi-objective scenario-based methodology, Transportation Research Part C: Emerging Technologies 35 (2013) 57–84.

[17] H. A. Blom, G. Bakker, Safety evaluation of advanced self-separation under very high en-route traffic demand, Journal of Aerospace Information Systems 12 (6) (2015) 413–427.

[18] B. Ye, M. Hu, J. F. Shortle, Collision risk-capacity tradeoff analysis of an en-route corridor model, Chinese Journal of Aeronautics 27 (1) (2014) 124–135.

[19] M.-H. Nguyen, S. Alam, Airspace collision risk hot-spot identification using clustering models, IEEE Transactions on Intelligent Transportation Systems 19 (1) (2017) 48–57.

[20] G. Moek, J. Smeltink, Post implementation collision risk assessment for RVSM in the Africa Indian Ocean Region, Tech. Rep. NLR-CR-2005-443, National Aerospace Laboratory NLR (08 2005).

[21] H. A. Abbass, S. Alam, A. Bender, MEBRA: multiobjective evolutionary-based risk assessment, IEEE Computational Intelligence Magazine 4 (3) (2009) 29–36.

[22] S. Alam, M. M. Hossain, F. Al-Alawi, F. Al-Thawadi, Optimizing lateral airway offset for collision risk mitigation using differential evolution, Air Traffic Control Quarterly 23 (4) (2015) 301–324.

[23] R. E. Machol, Thirty years of modelling mid-air collisions, Interfaces 25 (5) (1995) 151–172.

[24] F. Netjasov, M. Janic, A review of research on risk and safety modelling in civil aviation, Journal of Air Transport Management 14 (4) (2008) 213–220.

[25] M. Mitici, H. A. Blom, Mathematical models for air traffic conflict and collision probability estimation, IEEE Transactions on Intelligent Transportation Systems 20 (3) (2018) 1052–1068.

[26] D. Anderson, X. Lin, A collision risk model for a crossing track separation methodology, The Journal of Navigation 49 (3) (1996) 337–349.

[27] D. Hsu, The evaluation of aircraft collision probabilities at intersecting air routes, The Journal of Navigation 34 (1) (1981) 78–102.

[28] P. Brooker, Lateral collision risk in air traffic track systems: A 'post-Reich' event model, The Journal of Navigation 56 (3) (2003) 399–409.
[29] P. G. Reich, A theory of safe separation standards for air traffic control, Tech. Rep. 64041, Royal Aircraft Establishment RAE (1964).
[30] ICAO European and North Atlantic Office, Application of separation minima (NAT Doc 008), 1st Edition-Amendment (2020).
[31] ICAO, Manual on Airspace Planning Methodology for the Determination of Separation Minima (Doc 9689-AN/953), 1st Edition (1998).
[32] W. Semke, N. Allen, A. Tabassum, M. McCrink, M. Moallemi, K. Snyder, E. Arnold, D. Stott, M. G. Wing, Analysis of radar and ADS-B influences on aircraft detect and avoid (DAA) systems, Aerospace 4 (3) (2017) 49.
[33] T. Delovski, K. Werner, T. Rawlik, J. Behrens, J. Bredemeyer, R. Wendel, ADS-B over satellite the world's first ADS-B receiver in space (26-30 May, 2014, Porto Petro, Majorca, Spain).
[34] M. A. Garcia, J. Stafford, J. Minnix, J. Dolan, Aireon space based ADS-B performance model, in: Integrated Communication, Navigation and Surveillance Conference (ICNS), IEEE, 21-23 April, 2015, Herdon, VA, USA, pp. 1–10.
[35] T. Li, Y. Wan, A fuel savings and benefit analysis of reducing separation standards in the oceanic airspace managed by the New York air route traffic control center, Transportation Research Part E: Logistics and Transportation Review 152 (2021) 102407.
[36] EUR/SAM: "double unidirectionality" post-implementation risk assessment, Tech. Rep. NYVI-IDSA-INF-001-1.0-09 (2009).
[37] S. Alam, C. Lokan, H. Abbass, What can make an airspace unsafe? characterizing collision risk using multi-objective optimization, in: 2012 IEEE Congress on Evolutionary Computation, 2012, pp. 1–8.
[38] M. Xiao, K. Cai, H. A. Abbass, Hybridized encoding for evolutionary multi-objective optimization of air traffic network flow: A case study on china, Transportation Research Part E: Logistics and Transportation Review 115 (2018) 35–55.
[39] D. Chen, M. Hu, H. Zhang, J. Yin, K. Han, A network based dynamic air traffic flow model for en-route airspace system traffic flow optimization, Transportation Research Part E: Logistics and Transportation Review 106 (2017) 1–19.
[40] ICAO Cir 319, A Unified Framework for Collision Risk Modelling in Support of the Manual on Airspace Planning Methodology for the Determination of Separation Minima (DOC 9689) (2009).
[41] Y. Zhang, J. Shortle, L. Sherry, Methodology for collision risk assessment of an airspace flow corridor concept, Reliability Engineering & System Safety 142 (2015) 444–455.
[42] P. Brooker, Longitudinal collision risk for ATC track systems: a hazardous event model, The Journal of Navigation 59 (1) (2006) 55–70.
[43] S. L. Hockaday, A. Chatziioanou, An analytical method for aircraft collision risk estimation, Transportation Research Part B: Methodological 20 (5) (1986) 415–428.
[44] ICAO, Procedures for Air Navigation Services - Air traffic management (Doc 4444), 17th Edition (2020).
[45] X. Lin, N. Fulton, M. Westcott, Target level of safety measures in air transportation-review, validation and recommendations, in: Proceedings of the IASTED International Congress on Advances in Management Science and Risk Assessment, Beijing, China, 2009, pp. 222–662.
[46] G. Moek, J. Smeltink, Revised pre-implementation collision risk assessment for RVSM in the Africa Indian ocean region, Tech. Rep. NLR-CR-2007-637, National Aerospace Laboratory NLR (2007).
[47] G. Moek, E. Lutz, W. Mosberg, Risk assessment of RNP10 and RVSM in the SAT FIR, Tech. Rep. 20899, ARINC Proprietary (2001).
[48] ICAO, Manual on the Implementation of Performance-based Longitudinal Separation Minima (Doc 10120), 1st Edition (2020).
[49] Risk assessment of RNP10 and RVSM in the south Atlantic flight identification regions including an assessment for limited implementation of RVSM on RN741, Tech. Rep., ARINC Incorporated (2001).
[50] ICAO, The thirteenth meeting of the regional airspace safety monitoring advisory group (RASMAG/13), RASMAG/13-WP/12 (2010).
[51] ICAO, The seventeenth meeting of the regional airspace safety monitoring advisory group (RASMAG/17), RASMAG/17-WP/21 (2012).
[52] Q. Cai, H. Ang, S. Alam, A multiobjective optimization approach for reducing air traffic collision risk, in: 2021 IEEE Congress on Evolutionary Computation (CEC), IEEE, 2021, pp. 1759–1766.
[53] ICAO Asia/Pacific Region, En-route Monitoring Agency (EMA) Handbook, 2nd Version (2010).

Appendix

Calculation of Lateral Overlap Probability

According to ICAO documents, there are two models for calculating the lateral overlap probability, i.e., $P_y(S_y)$. Those two models are respectively shown below.

The first model (M1) calculates $P_y(S_y)$ using the following equation:

$$P_y(S_y) = \int_{-\lambda_y}^{\lambda_y} \int_{-\infty}^{\infty} f_y(y_1) f_y(S_y + y_1 - y)\, dy_1 dy \approx 2\lambda_y \int_{-\infty}^{\infty} f_y(y_1) f_y(S_y + y_1)\, dy_1 \qquad (11)$$

where $f_y(y_1)$ is the probability density function for the lateral deviation y_1. The probability distribution of $f_y(y_1)$ is calculated as

$$f_y(y_1) = (1-\alpha)\frac{1}{2a_1} e^{-\frac{|y_1|}{a_1}} + \alpha \frac{1}{2a_2} e^{-\frac{|y_1|}{a_2}} \qquad (12)$$

in which α represents the percentage of aircraft that experience anomalies caused by aircraft navigation system errors.

In the above equation, the value of α is estimated as $\alpha = 1 - 0.05^{1/n}$ with n being the annual number of flights [49]. The parameter a_1 is determined by the RNP specification and is estimated as $a_1 = -\mathrm{RNP}/\ln 0.05$, while parameter a_2 is estimated as $a_2 = S_y$.

The second model (M2) calculates $P_y(S_y)$ using the following equation:

$$\mathrm{P_y(S_y)} = \left(\frac{2\alpha\lambda_y}{\beta_2}\right) e^{-\frac{S_y}{\beta_2}} \qquad (13)$$

where β_2 is the unauthorised lateral deviation of 10 NM, and α is the weight of the a-typical lateral error of the overall distribution and it is estimated as

$$\alpha = \frac{\lambda(k)}{M.e^{-\frac{|15|}{S_y}}} \qquad (14)$$

in which *M* is defined as the cumulative 12-month traffic counts. $\lambda(k)$ is the intensity parameter and is dependent of parameter *k* which is the cumulative 12-month total number incident of large lateral deviation. The relationship between λ and *k* is as follow:

$$0.95 = e^{-\lambda}\frac{\lambda_k}{k!} \qquad (15)$$

In this research, the parameter of *M* is set to be 72250 and the cumulative 12-months total number of large lateral deviations is 4, i.e., k = 4, based on the lateral deviation report for 2018. A detailed derivation of the formula used can be found in [53].

Calculation of Vertical Overlap Probability

The probability of vertical overlap of aircraft nominally flying at the same flight level on laterally adjacent flight paths, viz., $P_z(0)$, is calculated as

$$P_z(0) = \int_{-\lambda_z}^{\lambda_z} \int_{-\infty}^{\infty} f_z(z_1) f_z(z_1 - z)\, dz_1 dz \approx 2\lambda_z \int_{-\infty}^{\infty} f_z(z_1) f_z(z_1 - z)\, dz_1 \qquad (16)$$

where $f_z(z_1)$ is the probability distribution function of the vertical deviation z_1. Note that the vertical deviation is mainly caused by ASE and AAD. Let $f^{ASE}(z)$ and $f^{AAD}(z)$ respectively be the probability distribution functions of the ASE and AAD. Then $f_z(z_1)$ is calculated as

$$f_z(z_1) = \int_{-\infty}^{\infty} f^{ASE}(z) f^{AAD}(z_1 - a) da \qquad (17)$$

where $f^{AAD}(\mathrm{z})$ follows a double exponential distribution given as $f^{AAD}(\mathrm{z}) = \frac{1}{\sigma_{AAD}\sqrt{2}} \exp\left(-|z|\sqrt{2}/\sigma_{AAD}\right)$.

In order to estimate $f^{ASE}(a)$ involved in equation 14, it is assumed that there are n_{AT} different types of aircraft operating in a given RVSM airspace. Each type of aircraft have their own parameters subject to the ASE variability of all the airframes and each type have their own ASE probability distributions $f_i^{ASE}(a), i = 1, \ldots, n$. An overall ASE probability density $f^{ASE}(a)$ for the full RVSM aircraft population is calculated as a weighted mixture of the ASE distribution by different types of aircraft, i.e.,

$$f^{ASE}(a) = \sum_{i=1}^{n_{AT}} \beta_i f_i^{ASE}(a) \qquad (18)$$

in which the weighing factor β_i is the proportion of flight time contributed by each aircraft type.

Both the weighting factors and the ASE probability distributions required are derived from the monitoring data with regards to a given RVSM airspace. The data can be collected by ground-based Height Monitoring Units (HMUs) or by air portable GPS Monitoring Units (GMUs). Based on monitoring data, $f_i^{ASE}(a)$ is observed to follow the gaussian double exponential distribution given as

$$f^{ASE}(a) = (1-\alpha_i)\frac{1}{\sigma_{1_i}\sqrt{2\pi}}\mathrm{e}^{-\frac{1}{2}\left(\frac{a-\mu_i}{\sigma_{1_i}}\right)^2} + \alpha_i\frac{1}{\sigma_{2_i}\sqrt{2\pi}}\mathrm{e}^{-\frac{|a-\mu_i|\sqrt{2}}{\sigma_{2_i}}} \qquad (19)$$

Calculation of Occupancy

There are 2 types of occupancy, namely same direction occupancy and opposite direction occupancy. To determine the occupancy, the number of proximate aircraft pairs for pairs of parallel routes have to be determined first. Every flight on its route is compared with other flights that are on the adjacent parallel route by using the reporting points. The reporting points used must be points that are at a right angle to the plane of the parallel routes so as to compare the passing time of aircraft on one route to the passing time of aircraft on the other route and they can be the waypoints or interpolated points between the waypoints that have timestamps. For Singapore procedural airspace, the reporting points used for parallel route pair N892-L625 are MABLI and LUSMO and the reporting points used for parallel route pair N884-M767 are LAXOR and TEGID.

If two flights are at the same flight level, then they are counted as an approximate pair as long as the time difference between any two reporting points for those two flights is less than or equal to 15 minutes (a time duration taken by a flight to fly S_x).

The number of proximate aircraft pairs for all route pairs is summed up after considering all the flights. The purpose of computing the number of proximate pairs is to determine $E_y(lateral\ occupancy)$. The occupancy is calculated as $E_y = 2n_y/n$, where n_y is the number of proximate aircraft pairs and n is the total number of aircrafts in the parallel route pairs.

Calculation of Horizontal Overlap Probability

The horizontal overlap probability for a pair of aircraft with speeds V_1 and V_2 at a given time point t is calculated as

$$HOP(t|V_1,V_2) = \frac{\pi\lambda_{xy}^2}{16\lambda^2}e^{-|D_x(t)|/\lambda}\left(\frac{|D_x(t)|}{\lambda}+1\right) \qquad (20)$$

where $D_x(t) = (V_1 - V_2)t - \hat{d}_1^0 + \hat{d}_2^0$ is the distance between two aircraft and λ is the scale parameter of the along- track and cross-track error distributions. The along-track and cross-track errors are assumed to follow a double exponential distribution.

Distribution of Speed Variation

The notations of $f_1(V_1)$ and $f_2(V_2)$ in the longitudinal risk model are the probability distribution functions for the aircraft speed variations. It is assumed that both $f_1(V_1)$ and $f_2(V_2)$ follow a double exponential distribution with scale parameter $\lambda_v = 5.82\ knots$. The assumed average aircraft ground speed of 480 knots is used as the location parameter V_0. The double exponential distribution is truncated at 100 knots on either side of the location parameter, and then normalized to equal 1. Thus, $f_1(V_1)$ and $f_2(V_2)$ have the same form as follows

$$f_1(V_1) = \frac{1}{2\lambda_v}e^{-\frac{|V-V_0|}{\lambda_v}}, -100 \le V_1 \le 100 \qquad (21)$$